Degradable multi(aryl azide) star copolymer as universal photo-crosslinker for elastomeric scaffolds

Louis Gangolphe, Stéphane Dejean, Audrey Bethry, Sylvie Hunger, Coline Pinese, Xavier Garric, Frédéric Bossard, Benjamin Nottelet

Degradable multi(aryl-azide) star copolymer as universal photo-crosslinker for elastomeric scaffolds

Louis Gangolphe[a,b], Stéphane Déjean[a], Audrey Bethry[a], Sylvie Hunger[a], Coline Pinese[a], Xavier Garric[a], Frédéric Bossard[b], Benjamin Nottelet[a]*

[a]*Department of Artificials Biopolymers, Max Mousseron Institute of Biomolecules (IBMM), UMR CNRS 5247, University of Montpellier, France*

[b]*Univ. Grenoble Alpes, CNRS, Grenoble INP*, LRP, 38000 Grenoble, France * Institute of Engineering Univ. Grenoble Alpes*

[*]*benjamin.nottelet@umontpellier.fr*

Abbreviations: polyhydroxybutyrate-co-hydroxyvalerate (PHBV); 2,6-bis(azidobenzylidene)-4-methylcyclohexanone (BA); poly(methyl methacrylate) (PMMA); polybutadiene (PB); poly(lactide) (PLA); poly(ethylene glycol methacrylate)-PLA (PEGMA-PLA); poly(ethylene glycol) (PEG); 8-arm poly(ethylene glycol) (tripentaerythritol) ($PEG_{8arm}10k$); poloxamer (Pluronic®F127); tin(II) 2-ethylhexanoate ($Sn(Oct)_2$); dichloromethane (DCM); diethylether (Et_2O); N,N-dicyclohexyl-carbodiimide (DCC); 4-(dimethylamin)pyridine (DMAP); N,N-dimethylformamide (DMF); tetrahydrofuran (THF); PLA_{50}-Pluronic®-PLA_{50} ($PLA_{50}PLU$); $PEG_{8arm}10k$-PLA_{94} (s-PLA); $PEG_{8arm}10k$-PLA_{94}-fN3 (s-PLA-fN3); average molecular weights ($\overline{Mn}$); dispersities (Đ); size exclusion chromatography (SEC); nuclear magnetic resonance (NMR); deutered chloroform ($CDCl_3$); dimethyl sulfoxide (DMSO-d6); tetramethylsilane (TMS); differential scanning calorimetry (DSC); scanning electron microscope (SEM); mercury bulb (MB); metal halide bulb (MHB); Fetal Bovine Serum (FBS); Young modulus (E); stress at yield (σ_y); strain at yield (ε_y); stress at break (σ_{break}); strain at break (ε_{break}); sodium bicarbonate (Na_2CO_3); magnesium sulfate ($MgSO_4$); phosphate buffered saline (PBS); initial weight (Wi); weight of the wet samples (Ww), weight dry after x time (Wx); DiButyldithioCarbamate (ZDBC); Lactate Dehydrogenase (LDH).

Abstract

Degradable elastomers with elastic properties close to those of soft-tissues are necessary for tissue-engineering. Most degradable elastomers developed so far are based on the use of functional low molecular weight pre-polymers that are associated with molecular crosslinkers to yield the elastomeric 3D networks. To overcome this limitation, we present in this work the concept of star-shaped macromolecular multi(aryl-azide) photo-crosslinker that has the ability to efficiently crosslink any polymer containing C-H bonds independently of its molecular weight and without the need for pre-functionalization. This concept of universal crosslinking agent is illustrated with a star-shaped copolymer composed of 8-arm poly(ethylene glycol) core and poly(lactide) side arms functionalized with aryl-azide moieties (PEG_{8arm}-PLA-fN_3). It was selected to yield electrospun photo-crosslinked scaffolds, where its macromolecular nature allows for a smooth process while making possible to fit its chemical nature with the one of the polymer matrix. A parameter study is first carried out on PEG_{8arm}-PLA-fN_3 / PLA-Pluronic®-PLA films to evaluate the impact of the polymers molecular weight, polymers ratios, and UV irradiation conditions on the crosslinking efficiency. This study confirms that high crosslinking efficiencies can be obtained with PEG_{8arm}-PLA-fN_3 (60%) compared to commercial bis(aryl-azide) photo-crosslinker (15%). Best conditions are then used to yield electrospun microfibers(1-2 µm) crosslinked with PEG_{8arm}-PLA-fN_3 resulting in biocompatible and highly elastomeric scaffolds ($\varepsilon_y > 100\%$) compared to uncrosslinked scaffolds($\varepsilon_y < 10\%$). In addition, we show that degradation rate can be controlled over time depending on the blend content of PEG_{8arm}-PLA-fN_3. Taken together, these results demonstrate the potential and usefulness of macromolecular multi(aryl-azide) photo-crosslinkers to develop original degradable elastomeric scaffolds for soft-tissue reconstruction.

Keywords:

Degradable elastomers, Tissue engineering, Electrospinning, UV photo-crosslinking, Scaffolds

1 Introduction

A large number of researches deal with elastomeric biomaterials based on synthetic polyesters for soft tissue engineering[1,2]. These (bio)resorbable materials solve the problem associated with biostable materials, whose long term fate is generally in question, while producing minimal long-term inflammation[3]. Currently, chemically crosslinked elastomers receive much attention due to numerous specific properties of interest for soft tissue engineering including 1) a linear degradation preserving mechanical properties and 3D structure of the materials over time; 2) the possibility to reach high Young's modulus; and 3) a limited crystallinity coming from less oriented polymeric chains, improving cell colonization and lowering the inflammatory response[4]. Through all chemically crosslinked elastomers based on polyesters, thermo-crosslinking (radical and condensation reactions[5]), click-chemistry (Diels-Alder cyclo addition[6–8], 'thiol-Michael addition'[9], thiol-yne 'click'[10]) and photo-crosslinking [11–16] are the major post-treatments used to produce (bio)resorbable 3-dimensional (3D) networks.

A particular interest has been paid to photo-crosslinking due to its advantages such as easy implementation, lower thermal energy production and fast processing for further industrial development[17]. This method requires at least two photo-crosslinkable pendant or chain-end groups (eg. acrylate), and a photo-initiator[18]. Lately, research has focused on the development of new biocompatible photo-initiators and photo-crosslinking agents to increase the crosslinking efficiency and to modulate elastomers' mechanical and degradation properties[19]. In this respect, Rupp *et al.* [20] reported on the preparation of a photo-crosslinked elastomer generated from the non-functional (polyhydroxybutyrate-co-hydroxyvalerate (PHBV)) thanks to the use of the bis(aryl-azide) 2,6-bis(azidobenzylidene)-4-methylcyclohexanone (BA) (Figure 1). This strategy relies on the UV-activation of the aryl-azide group to generate highly reactive nitrene species (Scheme 1) that can insert into carbon-hydrogen bonds of the polymer backbone, and thus lead to crosslinking via amine groups. The main advantages of this approach are i) that any polymer containing CH bonds can potentially be crosslinked and ii) that crosslinking efficiency should be largely independent of the polymer molecular weight. Besides PHBV, this UV-reactive crosslinker has been recently employed with other polymers including poly(methyl methacrylate) (PMMA) or polybutadiene (PB) [21–24]. However, the outcome of the cited studies is unclear with results that do not corroborate. Even though this approach could be an elegant and straightforward way to produce polyester-based elastomers without polyester-chain's functionalization or functional lactone synthesis, to our knowledge, no study has been

conducted on the design of elastomers based on medically relevant degradable polyesters like poly(lactide) (PLA), poly(ε-caprolactone) and copolymers thereof. This may be due to the low crosslinking efficiency that seems indeed associated with such bis(aryl-azide) photo-crosslinkers. In an attempt to increase the crosslinking efficiencies, other strategies take benefit from macromolecular architectures to yield multifunctional macromolecular crosslinkers. This is for example the case of Xie *et al.* who reported the use of methacrylated star-shaped PLA to generate PEGMA-PLA 3D network upon UV irradiation[25,26]. Consequently, developing aryl-azide multifunctional degradable photo-crosslinker based on star-block PEG-PLA copolymers (Scheme 1) appears as a convenient way to overcome the possible limitation of the bis(aryl azide) crosslinking while adding control over the final elastomer's degradation rates.

Another limiting point to consider in the search for photo-crosslinked degradable elastomers for soft tissues scaffolding, is the spatial limitation of photo-crosslinking. According to Avadenei *et al.*[21], azide cross-linking agent is restricted to micro-scale materials. Among a wide range of process to build architected materials dedicated to soft-tissue reconstruction[27–30], electrospinning process that produces micro/nano-scale fibers appears therefore as the most appropriate choice to build scaffolds using aryl-azide crosslinker. Combining aryl-azide crosslinker and electrospinning may be very promising to yield novel biomaterials able to mimic the structure and the properties of soft-tissues[31]. To date, association of photo-irradiation and electrospinning has been mainly limited to functionalization of nanofibers using click chemistry [32,33], and to the best of our knowledge, only few studies were conducted to produce fibrous scaffolds based on photo-crosslinked fibers[34–36]. Thus, electrospinning process could benefit from multi(aryl-azide) crosslinking agent in an effort to create a new generation of elastomeric scaffolds based on photo-crosslinked fibers.

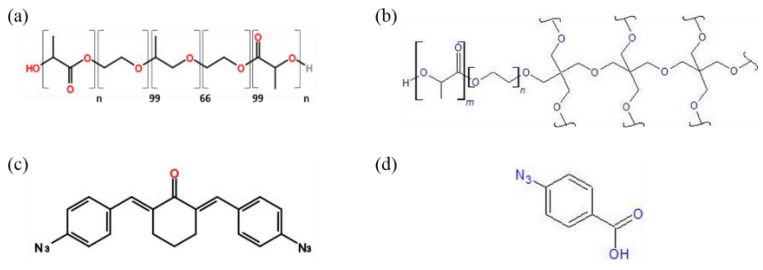

Figure 1: Chemical structures of (a) PLA_{50}-Pluronic®-PLA_{50} triblock copolymer; (b) PEG_{8arm}10k-PLA 8-armed star-block copolymer; (c) 2,6-bis(azidobenzylidene)-4-methylcyclohexanone (BA); (d) 4-azidobenzoic acid.

Based on the aforementioned considerations, the present work aims 1) to clarify the real potential of 2,6-bis(azidobenzylidene)-4-methylcyclohexanone (BA) as photo-crosslinker; 2) to synthesize and evaluate the performance of a multifunctional (aryl azide) photo-crosslinker based on 8-armed star-block PEG-PLA ($PEG_{8arm}10k\text{-}PLA_{94}$ -fN_3); 3) to validate the possibility to produce by electrospinning photo-crosslinked elastomeric fibrous scaffolds. For this, a particular focus is given to the triblock copolymer (PLA-Pluronic®-PLA) that has shown potential as a thermoplastic material for ligament tissue engineering and would be a valuable non-functional polymer to generate elastomers for soft tissue engineering applications[37–39].

To achieve this goal, in a first part crosslinking efficiency is discussed with respect to the following key parameters: PLA-Pluronic®-PLA molecular weight, aryl-azide crosslinker concentration, molecular bis-(aryl azide) vs. macromolecular octa-(aryl azide) crosslinkers, UV-irradiation conditions and polymer film thickness. As a main outcome of this study, we propose the development of elastomeric scaffolds for soft-tissue reconstruction based on photo-crosslinked high molecular weight PLA-Pluronic®-PLA fibers that are evaluated in terms of mechanical properties, degradation properties and cytocompatibilty.

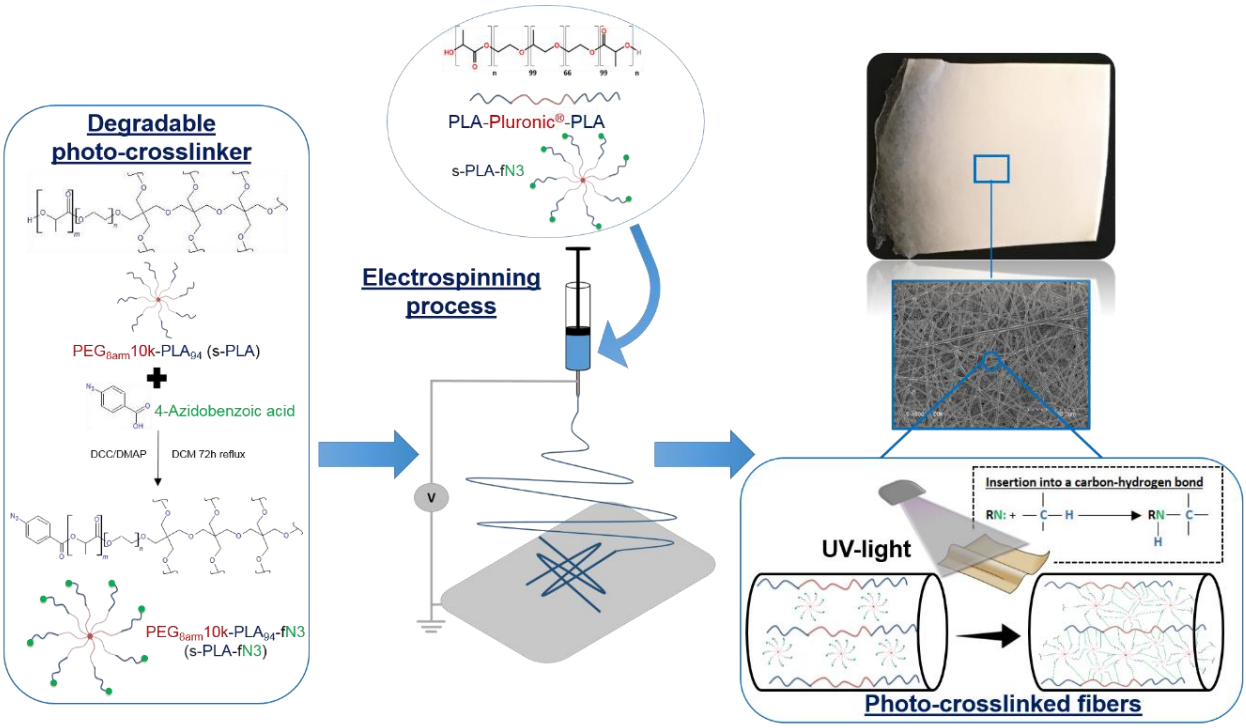

Scheme 1: Design concept of elastic micro-fibrous scaffolds based on degradable multi(aryl-azide) photo-crosslinkers.

2 Materials and methods

2.1 Materials

D,L-lactide and L-lactide were purchased from Purac (Lyon, France). 8-arm Poly(ethylene glycol) (tripentaerythritol) (PEG_{8arm}10k, Mw = 10 000 $g.mol^{-1}$) was purchased from JenKem Technology Co., Ltd (Beijing, China). Poloxamer (Pluronic®F127, Mw = 12 600 $g.mol^{-1}$), tin(II) 2-ethylhexanoate ($Sn(Oct)_2$, 95%), dichloromethane (DCM), diethylether (Et_2O), N,N-dicyclohexyl-carbodiimide (DCC), 4-(dimethylamin)pyridine (DMAP) and N,N-dimethylformamide (DMF), tetrahydrofuran (THF) were purchased from Sigma-Aldrich (St Quentin Fallavier, France). 2,6-Bis(4-azidobenzylidene)-4-methylcyclohexanone (BA) and 4-azidobenzoic acid were bought from TCI (Paris, Europe). All chemicals were used without further purification with exception of DCM and DCC. DCM was dried over calcium hybrid and freshly distillated before use. DCC was solubilized in anhydrous DCM with $MgSO_4$, stirred during 6 hours, then filtered and dried before use.

2.2 Characterization

FT-IR spectra of polymer films were recorded with a Perkin Elmer Spectrum 100 spectrometer.

Average molecular weights ($\overline{Mn}$) and dispersities (Đ) were determined by size exclusion chromatography (SEC) Shimadzu using two mixed medium columns PLgel 5 µm MIXED-C (300 x 7.8 mm), Shimadzu RI detector 20-A and Shimadzu UV detector SPD-20A (370 nm^{-1}) (40°C thermostatic analysis cells). Tetrahydrofuran (THF) was the mobile phase with 1 $mL.min^{-1}$ flow at 30°C (column temperature). Polymer was dissolved in THF to reach 10 $mg.mL^{-1}$ concentration; afterwards, solution was filtered through a 0.45 µm Millipore filter before injection. $\overline{Mn}$ and Đ were expressed according to calibration using polystyrene standards.

^1H NMR spectra were recorded from an AMX Brucker spectrometer operating at 300 MHz at room temperature. The solvent used was deutered chloroform and DMSO-d6. The chemical shift was expressed in ppm with respect to tetramethylsilane (TMS).

Thermal properties of the polymers were analysed by differential scanning calorimetry (DSC) from a Perkin Elmer Instrument DSC 6000 Thermal Analyzer characterized of the different polymers. It was carried out under nitrogen. Samples were heated to 100°C (10°$C.min^{-1}$), then cooled to -50°C (10°$C.min^{-1}$), before a second heating ramp to 120°C (5°$C.min^{-1}$). Samples

based on $PEG_{8arm}10k\text{-}PLA_{94}$ were heated to 180°C (10°C.min^{-1}), then cooled to -50°C (10°C.min^{-1}), before a second heating ramp to 180°C (5°C.min^{-1}). Glass transition temperature (Tg) was measured on the second heating ramp.

Morphology of the samples was examined with a Hitachi S4800 Scanning electron microscope (Technology platform of IEM Laboratory of the Balard Chemistry pole) with an acceleration voltage of 2 kV and at magnifications X 500, X 1000 and X 5000 times with 3 images at each magnification.

2.3 Synthesis of copolymers

Triblock copolymer PLA_{50}-Pluronic®-PLA_{50} ($PLA_{50}PLU$) and $PEG_{8arm}10k\text{-}PLA_{94}$ (94% L-Lactic units and 6% D-Lactic units) (s-PLA) were synthesized by ring-opening polymerization (ROP) as described in a previous work [37]. For $PLA_{50}PLU$ three molecular weights were targeted 50 000, 100 000 and 200 000 g.mol^{-1}, with the corresponding copolymers being noted as $PLA_{50}PLU50$, $PLA_{50}PLU100$ and $PLA_{50}PLU200$, respectively. For $PEG_{8arm}10k\text{-}PLA_{94}$ an overall molecular weight of 20 000 g.mol^{-1} was targeted. For this, determined amounts of D,L-lactide, L-lactide and Pluronic®F127 or $PEG_{8arm}10k$ were introduced in a flask, to which $Sn(Oct)_2$ was then added (0.1 mol% with respect to D,L-lactide units). Argon-vacuum cycles were applied before sealing the flask under vacuum. ROP was carried out in an oven at 130°C for 5 days under constant stirring. Afterwards, the mixture was dissolved in DCM and precipitated in cold Et_2O. The final triblock copolymer was dried under reduced pressure to constant mass.

2.3.1 PLA_{50}-Pluronic®-PLA_{50}

^{1}H NMR (300 MHz; $CDCl_3$): δ (ppm) = 5.1 (q, 1H, CO–C*H*-(CH_3)–O), 3.6 (s, 4H, CH_2–CH_2–O), 3.5 (m, 2H, CH(CH_3)–CH_2–O), 3.4 (m, 1H, C*H*(CH_3)–CH_2–O), 1.5 (m, 3H, CO–CH(CH_3)–O), 1.1 (m, 3H, CH(CH_3)–CH_2–O). (Fig. A.1)

The copolymer molecular weight was determined using the equations (1) and (2) acknowledging a molecular mass of 72 g.mol^{-1}for the lactic unit.

(1) $\overline{DP}_{PLA} = \overline{DP}_{PEG} * (I5.1PLA\ \ peak\ integration / I3.6PEG\ \ peak\ integration)$

(2) $\overline{Mn} = 2 * \left(\overline{DP}_{PLA} * 72\right) + \overline{Mn}_{Pluronic\ F127}$

2.3.2 $PEG_{8arm}10k\text{-}PLA_{94}$

^{1}H NMR (300 MHz; $CDCl_3$): δ (ppm) = 5.1 (q, 1H, CO–C*H*-(CH_3)–O), 4.3 (m, 2H, O-CH_2-C-C*H*$_2$-O), 3.6 (s, 4H, C*H*$_2$–C*H*$_2$–O), 3.3 (m, 2H, O-C*H*$_2$-C-CH_2-O), 1.5 (t, 3H, CO-CH-(C*H*$_3$)-O). (Fig. A.2).

The copolymer molecular weight was determined using equations (1) and (3)

$$(3)\ \overline{Mn} = 8 * \left(\overline{DP}_{PLA} * 72\right) + \overline{Mn}_{\mathrm{PEG8arm10k}}$$

2.4 Aryl-azide functionnal $PEG_{8arm}10k\text{-}PLA_{94}$ (s-PLA-fN_3)

The 8-armed star-block copolymer $PEG_{8arm}10k\text{-}PLA_{94}$ ($\overline{Mn_{theo}}$ = 20 kg.mol^{-1}) was solubilized in freshly distilled DCM (20% w/v). Determined amounts of 4-azido benzoic acid (20 eq./chain), DCC (20 eq./chain) and DMAP (20 eq./chain) were added. The mixture was heated at 45°C for 6 days under stirring in the dark. The reaction medium was filtered and washed (three times) by an aqueous solution of Na_2CO_3 then dried with $MgSO_4$. The copolymer solution was precipitated in cold diethyl ether in the dark. The aryl-azide functionnal $PEG_{8arm}10k\text{-}PLA_{94}$-fN3 (s-PLA-fN3) was dried under reduced pressure to constant mass. The yield of functionalization was determined by comparing the integration of the aryl-azide characteristic signal at 8.0 and the integration of proton resonance at 4.2 ppm.

^{1}H NMR (300 MHz; DMSO-d6): δ (ppm) = 8.0 (d, 2H aromatic ring, C*H*=CH-C-N_3), 7.3 (d, 2H aromatic ring, CH=C*H*-N_3), 5.1 (q, 1H, CO–C*H*-(CH_3)–O), 4.3 (m, 2H, O-CH_2-C-C*H*$_2$-O), 3.6 (s, 4H, C*H*$_2$–C*H*$_2$–O), 3.3 (m, 2H, O-C*H*$_2$-C-CH_2-O), 1.5 (t, 3H, CO-CH-(C*H*$_3$)-O). (Figure 2)

2.5 Photo-crosslinking and gel content

For elastomers crosslinked with BA, PLA_{50}PLU copolymers with defined molecular weights were stirred in DCM with 2,6-bis(4-azidobenzylidene)-4-methylcyclohexanone (BA) (2-5 wt% of the polymer). For elastomers crosslinked with s-PLA-fN_3, PLA_{50}PLU copolymers with defined molecular weights were mixed with s-PLA-fN_3 at different weight ratios (10, 25 and 50 wt%) and stirred in DCM. For control, the same protocol was followed by replacing s-PLA-fN_3 by the non-functional s-PLA. Solutions were dried out in an aluminum mold to obtain thin films. Films were stored in a dark place for 24h. The resulting films were further dried under vacuum for 24h. Then, samples were irradiated under UV light (mercury or metal halide bulb; UV lamp emission spectrum in Fig. A.3) under inert atmosphere for different times with a

Dymax PC-2000 system (75 $mW.cm^{-2}$). For sake of clarity, in the rest of the text a 10 minutes irradiation time corresponds to 5 minutes of irradiation per side of the film. The distance measured between the bulb and samples was 13.5 cm and, within the enclosure, the temperature was recorded over the photo-crosslinking procedure (Fig. A.4). Intensity of radiation doses was evaluated using ACCU-CAL^{TM} 50 system. Later, elastomer films were cut, weighed and put in DCM (10 mL). After three washes, the insoluble crosslinked parts were removed from DCM and dried under vacuum during 24h. Finally, samples were weighed to determine the gel fraction according to equation (4):

$$(4)\ Gel\ fraction\ (\%) = (Weight\ of\ insoluble\ cross-linked\ parts / Weight\ of\ initial\ sample) * 100$$

2.6 Electrospun polymer solutions

Polymer blends $PLA_{50}PLU$ and s-PLA-fN_3 or s-PLA (90/10 , 75/25 and 50/50 w/w noted 90/10, 75/25 an 50/50 in the rest of the text, respectively) were dissolved in DCM/DMF (50/50 v/v)[40]. Blend concentrations were chosen to produce fibers without beads (90/10 : 14wt%, 75/25 : 18wt%, 50/50 : 22wt%). All mixtures were mechanically stirred at room temperature overnight, until total dissolution[41].

2.7 Electrospinning process

Electrospinning process was carried out with a horizontal syringe pump device. A high voltage power supply was set at 12-15 kV. Polymer solutions filled a 10 mL syringe with a 21-gauge needle (inner diameter 0.82 mm). Feed rate (2.1 mL/h) was controlled with the syringe pump (Fresenius Vial Program 2 IEC). The collector was a square aluminum foil and located 15 cm from the needle tip. Experiments were performed at room temperature. The fibrous scaffold was collected after 40 minutes of electrospinning. It was dried overnight before further experiments.

2.8 Photo-crosslinking of fibrous scaffolds

To guaranty low temperature inside the enclosure and maintain the morphology of the fibers, fibrous scaffolds were irradiated under UV light (mercury bulb) and inert atmosphere for 2 seconds at a frequency of 0.5 Hz. The sequential flashes were applied for determined periods

using a Dymax PC-2000 system (75 mW.cm^{-2}). The distance, the intensity of irradiation and the gel fraction were measured using the protocol described for films.

2.9 Mechanical properties

Tensile mechanical tests were carried out on micro-fibers scaffold samples. Samples were cut (30 x 10 mm) and thickness was measured with a micrometer. Scaffolds were analyzed in triplicate at 37°C (dry and hydrated state) with an Instron 3344 with a deformation rate of 10 mm/min. Young modulus (E, MPa), stress at yield (σ_y, MPa), strain at yield (ε_y,%), stress at break (σ_{break}, MPa) strain at break (ε_{break},%) were expressed as the mean value of the three measurement.

2.10 Degradation study

Fibrous tests samples were cut (10 x 10 mm), weighed (Wi = initial weight) and placed in 5 mL of phosphate buffered saline (PBS) (pH 7.4) at a constant temperature (37°C) under stirring. At different time points, fibrous materials were removed from PBS, weighed (Ww = weight of the wet samples), then dried to constant mass (Wx = weight dry after x time in PBS). The remaining mass of the samples was calculated from equation (5).

$$(5)\ Remaining\ mass\ (\%) = (1 - ((Wi - Wx)/Wi)) * 100$$

Water uptake was determined from equation (6)

$$(6)\ Water\ uptake\ (\%) = ((Ww - Wi)/Wi) * 100$$

2.11 Cytotoxicity assay

Cells and control polymer films were chosen in accordance with ISO 10993-5 guidelines. Mouse fibroblasts L929 cells (ECACC 85011425) were maintained in DMEM high glucose supplemented with 5% Fetal Bovine Serum (FBS), 2mM L-glutamine and 1% penicillin/streptomycin and cultured at 37°C and 5% CO2. Cells were tested to be free of mycoplasms. Negative (RM-C High Density Polyethylene noted C-) and positive (RM-B 0.25% Zinc DiButyldithioCarbamate (ZDBC) polyurethane noted C+) control films were purchased from Hatano Research Institute (Ochiai 729-5, Hadanoshi, Kanagawa 257, Japan). Cytotoxicity was assessed on extracts. First, extractions were carried out at 0.1g per mL for 72h at 37°C

under sterile conditions on complete growth medium following ISO 10993-12 recommendations. L929 cells were seeded at 15.10^3 cells per well in a 96-well plate and allowed to attach overnight. The culture medium was then removed and discarded from the cultures and an aliquot of the fibers extract was added into each well. Aliquots of the blank, negative and positive controls were added into additional replicate wells (n=9). After 24h incubation under appropriate atmosphere, extract's cytotoxicity was assessed by Lactate Dehydrogenase (LDH) assay (Pierce), according to the manufacturer's instruction. Briefly, medium from well was transferred to a new plate and mixed with LDH Reaction Mixture. After 30 minutes of incubation at room temperature, absorbances at 490 nm and 680 nm were measured using a CLARIOstar® microplate-reader (BMG LABTECH's) to determine LDH activity.

The percentage of cytotoxicity were calculated from equation (7)

$$(7)\ Cytotoxicity\ (\%) = \left(\left((sample\ LDH\ activity) - \text{LDH-}\right)/(\text{LDH+"-"LDH-})\right) * 100$$

Where "LDH-"represents Spontaneous LDH Release Control (water-treated) and "LDH+" Maximum LDH Release Control activity obtained after cell lysis.

3 Results and discussion

3.1 Evaluation of molecular bis(aryl-azide) as photo-crosslinker

In order to prepare degradable elastomeric biomaterials starting from non-functional polyesters, we first focused on the triblock PLA_{50}-Pluronic®-PLA_{50} ($PLA_{50}PLU$). This family of copolymers showed promising properties for soft tissue engineering of ligaments due to their tunable degradation rate and their mechanical properties close to the natural tissue after processing to braided/twisted scaffolds[39]. The copolymers were prepared according to the procedure previously described[38] and are listed in Table 1. Targeted and experimental molecular weights (50 000, 100 000 and 200 000 $g.mol^{-1}$) were in agreements based on ^{1}H NMR spectra. Dispersities between 1.5 and 1.8 were determined by SEC analysis, which is in agreement with values classically obtained for the ROP of high molecular weight polyesters. These copolymers were further used to evaluate the real potential of 2,6-bis(azidobenzylidene)-4-methylcyclohexanone (BA) as photo-crosslinker. The three different triblock copolymers $PLA_{50}PLU50$, $PLA_{50}PLU100$ and $PLA_{50}PLU200$ were mixed with BA. The BA concentrations tested (2wt% and 5wt%) were chosen based on the data found in literature[20]. Gel fractions results (Fig. A.5) showed low crosslinking efficiency using BA as photo-crosslinker (gel fraction < 15%) despite a proven activation of aryl-azide. This was evidenced through the disappearance of the band at 2100 nm^{-1}, which is characteristic of the azide group (Fig. A.6). This lack of crosslinking despite aryl-azide photoactivation was attributed to the formation of azo-dimers and termination reactions that do not allow crosslinking[21]. Furthermore, molecular weight of the $PLA_{50}PLU$ copolymer did not influence significantly the crosslinking efficiency compared to nature of the UV-bulb used (metal halide bulb *versus* mercury bulb) and BA concentration. As expected, gel fraction increased with mercury bulb[42] and higher BA concentration (5%wt). However, crosslinking efficiency did not corroborate with other studies[20], where efficiencies up to 90% are reported against 15% here. This difference is due to the method used to evaluate the crosslinking efficiency. Whereas Rupp et al. used an indirect infrared spectrometric method based on the comparison of ester peaks' heights (measured at 1724 cm^{-1}) before and after photo-crosslinking, we chose to measure the gel fraction by weighing the remaining mass of material after solubilisation of the uncrosslinked chains for each sample, which is in our opinion a more appropriate and relevant method to accurately evaluate crosslinking extents. One could consider that the nature of the polymer to be crosslinked ($PLA_{50}PLU$ *vs.* PHBV) might be responsible for this low crosslinking. However,

other works[43], including unpublished data of our group, indicated high photo-insertion efficiencies of aryl-azide containing molecules into polyether-polyester copolymers.

Taking into account these results, we hypothesized that the limited functionality of BA (2 aryl-azide groups) associated to the direct proximity of the reactive groups on this small organic molecule could explain the poor outcome of BA-based crosslinking. As a consequence, BA was abandoned in the rest of this study and replaced by a multi(aryl-azide) macromolecular crosslinker.

Table 1: Molecular weight, dispersity and thermal properties of amorphous triblock copolymers PLA_{50}-Pluronic®-PLA_{50} (Pluronic®F127 used, $\overline{Mn_{theo}}$= 12 600 g.mol^{-1})

Sample name	Triblock copolymer	$\overline{Mn}_{NMR}$ (g.mol^{-1})	Đ	Tg (°C)	Tf (°C)	ΔHm (J.g^{-1})
PLA_{50}PLU 50	PLA_{50}-Pluronic®-PLA_{50}	47 600	1.51	11.1	/	/
PLA_{50}PLU 100	PLA_{50}-Pluronic®-PLA_{50}	99 100	1.59	23.4	/	/
PLA_{50}PLU 200	PLA_{50}-Pluronic®-PLA_{50}	203 000	1.82	31.1	/	/

3.2 Synthesis of a multi(aryl-azide) macromolecular photo-crosslinker (s-PLA-fN_3)

In order to prepare an elastomer based on multi(aryl-azide) photo-crosslinker, a low molecular weight 8-armed star-block copolymer, namely PEG_{8arm}10k-PLA_{94} (s-PLA), was synthesized (Fig. A.2). 8-arms copolymer was chosen to increase the number of reactive sites per molecule of crosslinker. Star PEG was selected as the core of the star copolymer to ensure a coherence of composition between the macromolecular crosslinker and the PLA_{50}-PLU. Semi-crystalline PLA_{94} arms were selected over amorphous PLA_{50} arms to enhance the expected elastomeric behavior thanks to the combination of crystalline nods and chemical crosslinks in the 3D network. s-PLA copolymer was prepared according to the procedure described by our group[37–39] (Table 2). Targeted and experimental molecular weights ($\overline{Mn_{theo}}$ = 20 000 g.mol^{-1}) were in good agreements as confirmed by the ^{1}H NMR spectra. A low dispersity of 1.1 was determined by SEC analysis.

Table 2: Molecular weight, dispersity and thermal properties of semi-crystalline star-block copolymers $PEG_{8arm}10k\text{-}PLA_{94}$. Thermograms used to determine the thermal properties are provided as supplementary data (Fig. A.7).

Sample name	Diblock copolymer	$\overline{Mn}_{NMR}$ (g.mol^{-1})	Đ	Tg (°C)	Tf (°C)	ΔHm (J.g^{-1})
s-PLA	$PEG_{8arm}10k\text{-}PLA_{94}$	19 300	1.1	-40	22.8	10.2
s-PLA-fN3	$PEG_{8arm}10k\text{-}PLA_{94}$-fN3	18 600	1,1	-36 / 34	nd[a]	nd

[a] not detected under the conditions of analysis

The star-block copolymer was further reacted with 4-azidobenzoic acid to yield the multi(aryl-azide) macromolecular crosslinker $PEG_{8arm}10k\text{-}PLA_{94}\text{-}fN_3$ (s-PLA-fN_3) (Figure 2-a). Experimental molecular weight calculated from the ^{1}H NMR spectra ($\overline{Mn}$ = 18 600 g/mol) and dispersity of Đ = 1.1 determined by SEC analysis showed that no degradation of the s-PLA copolymer occurred during the synthesis.

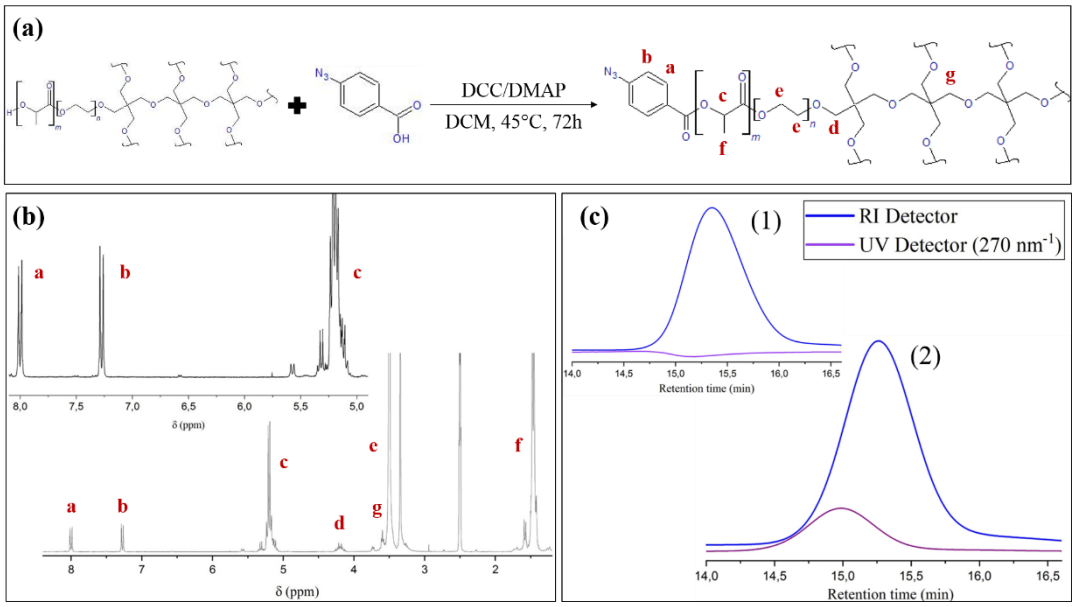

Figure 2: (a) Synthetic scheme of the degradable copolymer photo-crosslinker $PEG_{8arm}10k\text{-}PLA_{94}$-fN3 (s-PLA-fN3); (b) ^{1}H NMR spectra of $PEG_{8arm}10k\text{-}PLA_{94}$-fN3 (s-PLA-$fN_3$); (c) SEC analysis of (1) $PEG_{8arm}10k\text{-}PLA_{94}$ and SEC analysis of (2) $PEG_{8arm}10k\text{-}PLA_{94}$-fN3. UV detector (270nm^{-1}).

^{1}H NMR spectra of s-PLA-fN_3 is shown in Figure 2-b. Peaks at 8.0 and 7.3 ppm (peaks a and b) correspond to aromatic protons of the aryl-azide chain-end. The peaks at 5.2 ppm (peak c) and 1.5 ppm (peak f) correspond to the methine and methylene groups of the PLA backbone. The peaks at 4.3 ppm (peak d) were attributed to the tripentaerythritol core of the copolymers. Finally, peak at 3.3 ppm (peak e) was assigned to methylene groups of PEG. By comparison between the integrations of the peaks of the tripentaerythritol core and of the aryl-azide chain-ends a functionalization degree of 96% was calculated.

The grafting of 4-azidobenzoic acid onto s-PLA chain-ends was further confirmed by SEC analyses. After functionalization, a UV signal characteristic of aryl-azide groups (270 nm^{-1}) was visible at a retention time corresponding to the refractive index signal of the star-block copolymer (Figure 2-c-2). This was not the case for the starting s-PLA copolymer (Figure 2-c-1).

These results confirmed the successful chain-end functionalization of s-PLA with aryl-azide moieties, yielding the expected multi(aryl-azide) macromolecular photo-crosslinker s-PLA-fN_3.

3.3 Degradable elastomers photo-crosslinked by s-PLA-fN3

To evaluate the potential of s-PLA-fN3 for the preparation of degradable elastomeric biomaterials, we first focused on the influence of the PLA_{50}PLU molecular weight and the content of s-PLA-fN3 on the crosslinking efficiency. Based on the study carried out on bis(aryl-azide) photo-crosslinker, films having a thickness of 20 µm were prepared from PLA_{50}PLU(50-200)/s-PLA-fN3 blends at various compositions (90/10 , 75/25 and 50/50 w/w) prior to irradiation under UV-light for period 10 minutes (5 minutes for each side). Results are summarized in Figure 3.

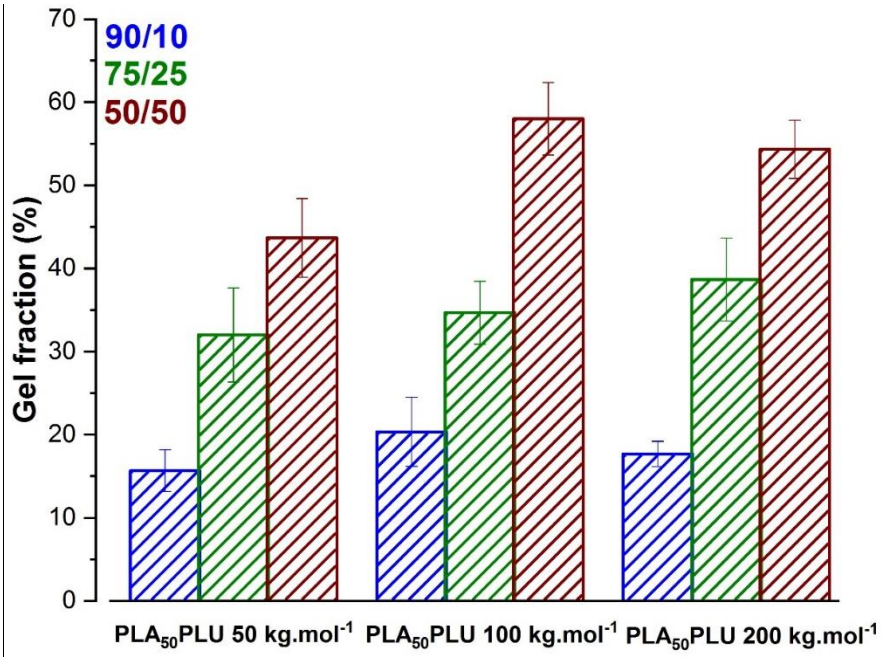

Figure 3: Influence of $PLA_{50}PLU$ molecular weight (50-200 $kg.mol^{-1}$) and of $PLA_{50}PLU$/s-PLA-fN3 weight ratios (90/10, 75/25 and 50/50) on the crosslinking efficiency evaluated by gel fraction analyses (20µm thick films, 5 minutes UV-irradiation per side. Data are expressed as means ± SD and correspond to measurements with n = 3).

As expected, the initial content of s-PLA-fN3 in the mixture had a strong influence on the crosslinking efficiency with gel fractions around 15%, 35% and 55% when s-PLA-fN3 ratios varied from 10 wt%, 25wt% and to 50wt%, respectively. On the opposite, the molecular weight of the $PLA_{50}PLU$ did not show any significant impact on the crosslinking efficiency. For a defined weight ratio of $PLA_{50}PLU$ (50-200)/s-PLA-fN3 gel fractions were similar whatever the $PLA_{50}PLU$ molecular weight. $PLA_{50}PLU$(50-200) are amorphous polymers with glass transition ranging from 11°C to 31°C (Table 1). At the temperature of UV crosslinking (Fig. A.4), chain mobility is higher for $PLA_{50}PLU50$ compared to $PLA_{50}PLU200$ but this higher mobility does not seem to significantly impact the crosslinking efficiency. Only at a 50/50 ratios, a slightly lower gel fraction was obtained for the $PLA_{50}PLU50$ compared to $PLA_{50}PLU100$ or $PLA_{50}PLU200$. This result might be due to a lower chain entanglement combined with higher chain mobility that partly prevent reaction between the active nitrene species and the polymeric chains[21]. It is to note that this independence of crosslinking efficiency over the molecular weight of the polymer is a unique feature considering the fact that most degradable elastomers are obtained from low molecular weight pre-polymers.

Kinetics of the photo-crosslinking were then followed over a 10 minutes period of time (Figure 4). After 2 minutes of UV-irradiation, the maximum gel fraction was already reached for most

$PLA_{50}PLU$/s-PLA-fN3 blends, which confirmed that aryl-azide photo-crosslinking is a very fast process [20], whatever the molecular weight of the $PLA_{50}PLU$ copolymer.

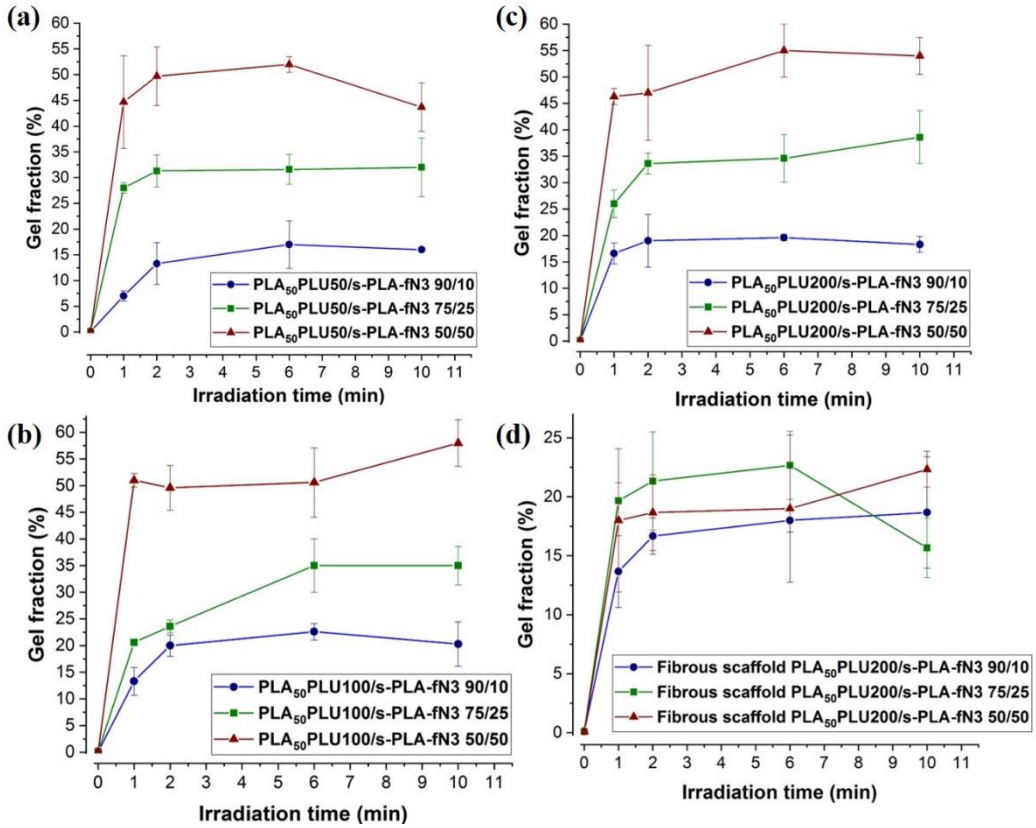

Figure 4: Crosslinking kinetics of the elastomers $PLA_{50}PLU$ (50-200)/s-PLA-fN3 evaluated by gel fraction. (a) $PLA_{50}PLU50$/s-PLA-fN3; (b) $PLA_{50}PLU100$/s-PLA-fN3; (c) $PLA_{50}PLU200$/s-PLA-fN3; (d) Crosslinking kinetics of the elastic microfibers scaffolds $PLA_{50}PLU$ (50-200)/s-PLA-fN3 evaluated by gel fraction. (Data are expressed as means ± SD and correspond to measurements with n = 3).

With aim to determine if the observed crosslinking could occur as a result of the photo-cleavage and chain radical rearrangement, control experiment was carried out. $PLA_{50}PLU$/s-PLA blends without aryl-azide groups, were irradiated under the same conditions. In the absence of aryl-azide groups, no gel fraction was obtained. This confirmed that 3D networks formation did not result from Norrish I/II type photo-cleavage and rearrangement [44], but was exclusively due to the insertion of active nitrene species on the polymeric chains. The evolution of the soluble fraction was also monitored over irradiation time. Corresponding chromatograms are provided in Figure 5. Before irradiation, the molecular weight distribution of both PLA_{50}-PLU200 and of s-PLA-fN3 are clearly identified. On the opposite, after just one minute of irradiation, a novel envelop is observed corresponding to population resulting from the degradation of PLA_{50}-PLU200 resulting from the Norrish I/II type photo-cleavage. This degradation continued with a decrease of molecular weight of the macromolecules of the soluble fraction with increasing

the irradiation time. This is in accordance with the results reported on BA-crosslinked PHBV[20].

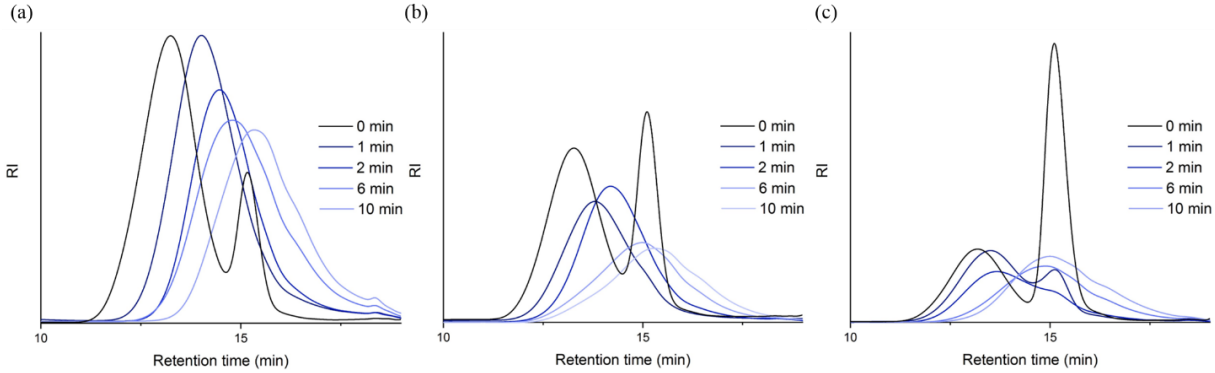

Figure 5: SEC analyses of the soluble fraction of the chemically crosslinked elastomers $PLA_{50}PLU200$/s-PLA-fN3 after as a function of the UV-irradiation time. (a) $PLA_{50}PLU200$/s-PLA-fN3 90/10; (b) $PLA_{50}PLU200$/s-PLA-fN3 75/25; (c) $PLA_{50}PLU200$/s-PLA-fN3 50/50.

Finally, the crosslinking efficiency of molecular bis(aryl-azide) photo-crosslinker BA and macromolecular multi(aryl-azide) photo-crosslinker s-PLA-fN3 with respect to the overall aryl-azide groups concentration in the blends were compared (Figure 6).

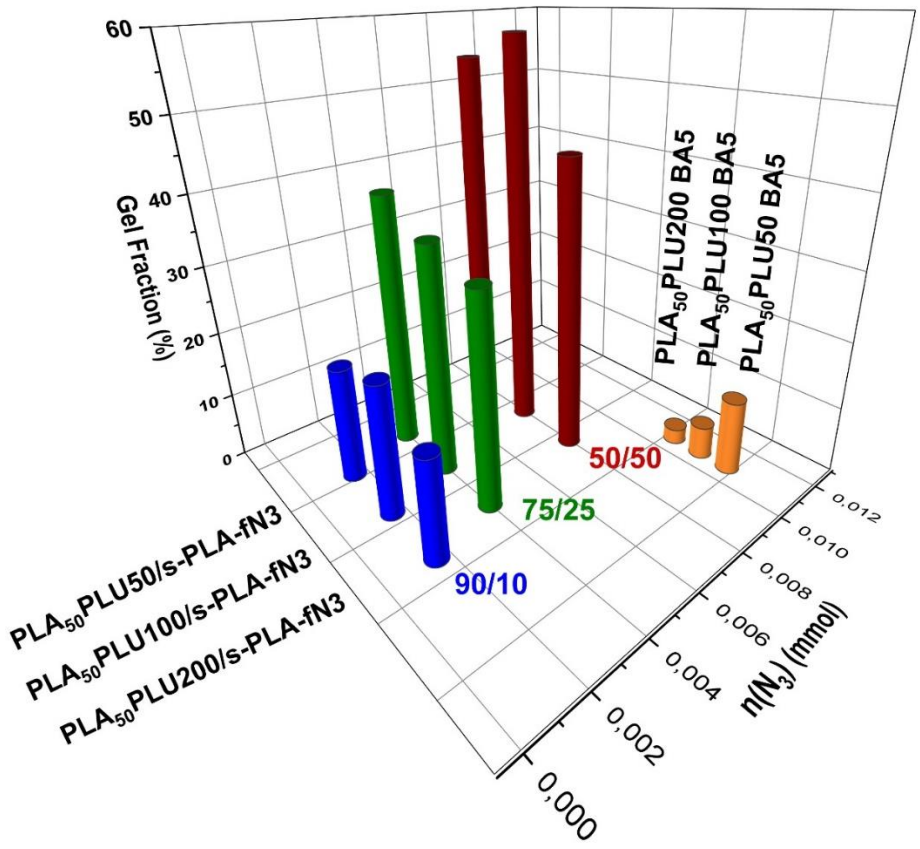

Figure 6: Gel fraction as a function of the nature of the aryl-azide photo-crosslinker (s-PLA-fN3 at 10, 25 and 50 wt% vs. BA at 5wt%) and the overall content of aryl-azide groups in the blend (n(N3)) (10 minutes irradiation time).

It is to note that the concentration of aryl-azide groups was higher in PLA_{50}PLU (50-200)-BA5 mixtures (5wt% of BA, 11 µmol) than in all PLA_{50}PLU/s-PLA-fN3 blends even when the highest concentration of s-PLA-fN3 (50wt%, 8 µmol) was used. However, gel fractions obtained were higher with macromolecular 8-branched star photo-crosslinker than BA, even for the lowest content of s-PLA-fN3 (10wt%, ca. 2 µmol), which corresponds to 5.5 times less photo-reactive moieties compared to 5wt% of BA. As expected, with 8 aryl-azide groups present on the s-PLA-fN3 star macromolecular photo-crosslinker, active nitrene species have more probability to be in contact with the PLA50PLU polymeric chain and to act as a crosslinking agent than the bi-functional BA. Moreover, reducing the mobility of the cross-linking agent due to its macromolecular nature and expected chains entanglement may also explain this enhanced efficiency of crosslinking.

3.4 Micro-scale scaffolds based on aryl-azide star-shaped PLA as photo-crosslinker

Based on the results obtained on films PLA_{50}PLU(50-200) that demonstrated a high potential of s-PLA-fN3 as photo-crosslinker, the next step was to evaluate the transferability of this approach into the electrospinning process to produce elastomeric and degradable scaffolds based on photo-crosslinked fibers. Having shown that the molecular weight of the PLA_{50}PLU copolymer does not influence the outcome, this next study was limited to PLA_{50}PLU200 that proved to be easily electrospun (data not shown). The same ratios of PLA_{50}-PLU200/s-PLA-fN3 (90/10, 75/25 and 50/50) were produced as described in the experimental section. Resulting scaffolds had a thickness of nearly 250 µm. To guaranty low temperature inside the enclosure (see experimental section and Fig. A.4 for more details) and maintain the morphology of the fibers, fibrous scaffolds were irradiated under UV light (mercury bulb) and inert atmosphere for 2 seconds at a frequency of 0.5 Hz. Various parameters have been investigated and are discussed in the following sections.

3.4.1 Fibers morphology

Fibers morphology was analyzed by SEM an typical images are shown in Figure 7. For a defined ratio, no difference in fiber diameter distribution was noticed between fibers based on s-PLA or s-PLA-fN3 even after UV-curing. In brief, all fiber diameters were in the range of 1 to 2 µm. The lowest fibers diameter (1.2 µm) was obtained with PLA_{50}-PLU200/s-PLA-fN3 90/10 blends and increased with the content of s-PLA-fN3 with fiber diameters of 1.65-1.98 µm and 1.74-2.13 µm for 75/25 and 50/50 blends, respectively. However, fiber distribution was more heterogeneous for the latter. It might be due to a non-total solvent evaporation that cause flatten fibers leading to interconnected fibers[45].

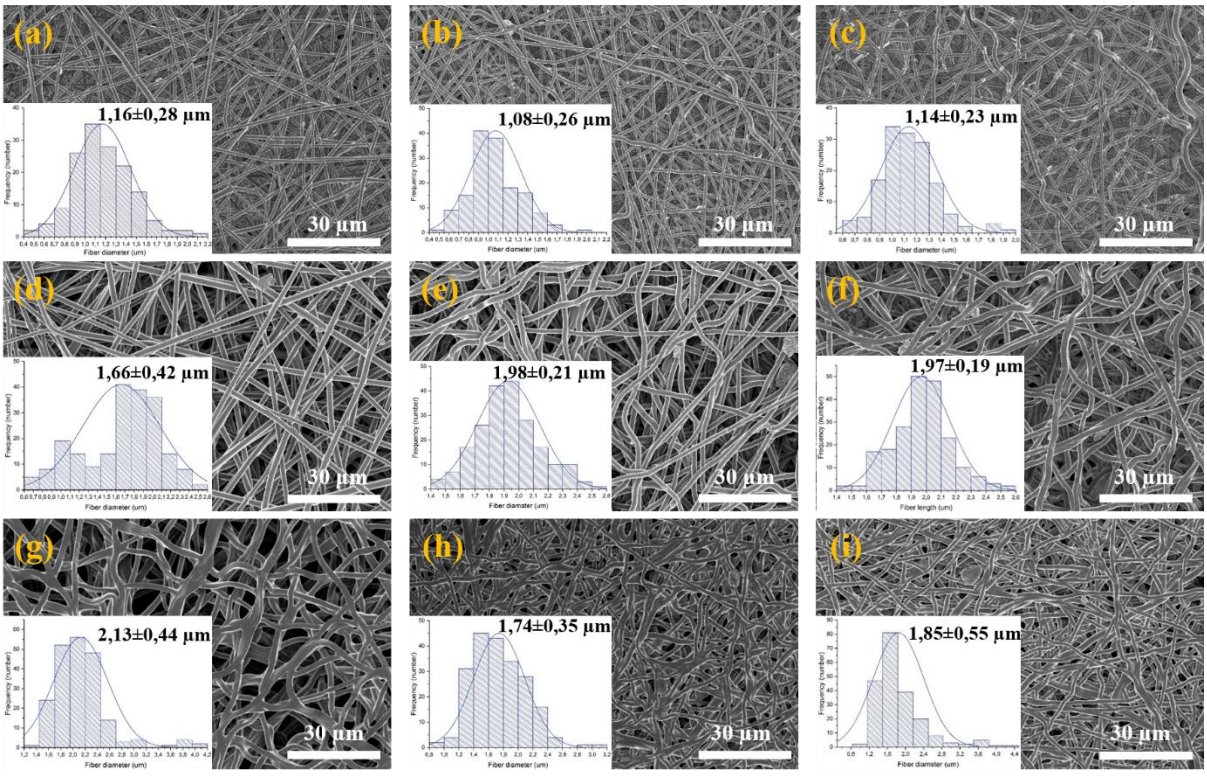

Figure 7: SEM images, microfiber diameter distributions of the different scaffolds based on PLA_{50}-PLU200/s-PLA and PLA_{50}-PLU200/s-PLA-fN3 (before and after 2 min of UV curing). Scale bar of SEM is 30 µm. (a) PLA_{50}-PLU200/s-PLA 90/10; (b) PLA_{50}-PLU200/s-PLA-fN3 90/10 uncured; (c) PLA_{50}-PLU200/s-PLA-fN3 90/10 UV-cured; (d) PLA_{50}-PLU200/s-PLA 75/25; (e) PLA_{50}-PLU200/s-PLA-fN3 75/25 uncured; (f) PLA_{50}-PLU200/s-PLA-fN3 75/25 UV-cured; (g) PLA_{50}-PLU200/s-PLA 50/50; (h) PLA_{50}-PLU200/s-PLA-fN3 50/50 uncured; (i) PLA_{50}-PLU200/s-PLA-fN3 50/50 UV-cured.

3.4.2 In-situ photo-crosslinking evaluation

In order to determine optimal UV-curing time to obtain an elastic micro-fibers scaffold, crosslinking study was conducted. Fibrous scaffolds based on PLA_{50}PLU200/s-PLA-fN3 under UV light (mercury bulb) and inert atmosphere for 2 seconds at a frequency of 0.5 Hz. After 2 minutes of UV-irradiation, the gel fraction obtained was maximal (20 – 25%) (Figure 4-d). This irradiation time was therefore selected for the rest of the studies. Values of gel fraction were lower for fibrous scaffolds (20-25%) than that of 20 µm films (15-65%). This may be due to both the thickness, ca. 250 µm, and opaque nature of the highly porous scaffolds, which may restrict UV penetration to few microns at the surface of the scaffolds. Considering UV barrier properties of aryl-azide compounds combined with s-PLA-fN3 polymer crystallinity, UV light might photo-cured fibers only on surface (few micrometers). Hence, no significant difference between fibrous scaffolds regardless of s-PLA-fN3 concentrations was noticed.

3.4.3 Mechanical properties

A major challenge in the field of synthetic resorbable materials, dedicated to soft tissue reconstruction, is to ensure the mechanical properties preservation of the biomaterial/host tissues complex over degradation and healing processes[46,47]. Therefore, PLA_{50}-PLU200/s-PLA-fN3 mechanical behaviors were evaluated under dry and hydrated state at 37°C (Table 3).

Table 3: Elastic microfibers scaffolds (FS) mechanical properties in the dry and hydrated state at 37°C. Young's modulus (E), ultimate stress (σ_{break}), ultimate strain (ε_{break}), and elastic limit (ε_y). (Data are expressed as means ± SD and correspond to measurements with n = 3).

Fibrous scaffolds blends	**Dry state**				**Hydrated state**			
	E (MPa)	$\boldsymbol{\varepsilon_y}$ (%)	$\boldsymbol{\sigma_{break}}$ (MPa)	$\boldsymbol{\varepsilon_{break}}$ (%)	E (MPa)	$\boldsymbol{\varepsilon_y}$ (%)	$\boldsymbol{\sigma_{break}}$ (MPa)	$\boldsymbol{\varepsilon_{break}}$ (%)
FS PLA50PLU200/ s-PLA-fN3 90/10	0.7 ± 0.1	12 ± 1	0.6 ± 0.1	174 ± 26	15.9 ± 1.5	5 ± 1	1.7 ± 0.2	117 ± 14
FS PLA50PLU200/ s-PLA-fN3 75/25	0.3 ± 0.1	182 ± 4	1.4 ± 0.3	333 ± 68	10.6 ± 1.0	3 ± 0	1.4 ± 0.1	176 ± 16
FS PLA50PLU200/ s-PLA-fN3 50/50	0.2 ± 0.0	115 ± 10	0.6 ± 0.0	257 ± 32	6.6 ± 2.3	3 ± 0	0.9 ± 0.2	89 ± 21
FS PLA50PLU200/ s-PLA 90/10	11.6 ± 2.5	3 ± 1	1.0 ± 0.1	120 ± 13	18.4 ± 4.5	3 ± 1	1.7 ± 0.4	101 ± 14

FS PLA50PLU200/ s-PLA 75/25	29.3 ± 1.3	1 ± 0	2.1 ± 0.3	171 ± 28	34.2 ± 14.6	1.7 ± 1	1.9 ± 0.3	97 ± 6
FS PLA50PLU200/ s-PLA 50/50	2.4 ± 0.9	7 ± 2	1.2 ± 0.2	146 ± 11	5.6 ± 0.3	3 ± 1	0.7 ± 0.0	93 ± 9

On the one hand, in a dry state at 37°C, non UV-cured fibrous scaffolds based on PLA_{50}PLU200/s-PLA the 75/25 ratio had the lower deformability with a high Young modulus (E = 29.3 MPa) and a low elastic limit (ε_y = 1.3%). The 50/50 ratio on the opposite was the most deformable material (E = 2.4 MPa and ε_y = 7.3%). Fiber diameters in the observed range (ca. 1-2 µm) did not influence mechanical properties in accordance with other studies [48,49]. On the other hand, in a dry state at 37°C, UV-cured fibrous scaffolds based on PLA_{50}PLU200/s-PLA-fN3 showed higher elastic properties (E = 0.22 – 0.68 MPa and ε_y = 12 – 182%) than non UV-cured fibrous scaffolds (E = 2.44 – 29.3 MPa and ε_y = 1.3 – 7.3%). A remarkable increase of elastic limit was therefore obtained thanks to the fibers crosslinking with quasi-linear stress-strain curves (Figure 8). It yielded scaffolds with lower ultimate stress (0.58 – 1.38 MPa for crosslinked FS *vs.* 1.01 – 2.01 MPa for the non-crosslinked) and much higher ultimate strain (174 – 333 % *vs*. 120 – 146 %). As expected, FS PLA_{50}PLU200/s-PLA-fN3 75/25 and 50/50 showed higher elastic properties (E = 0.22 – 0.34 MPa; ε_y = 115 - 182%) than 90/10 (E = 0.68 MPa; ε_y = 12%) confirming the interest of using the star-shaped macromolecular s-PLA-fN3 photo-crosslinker. It is to note that for similar crosslinking efficiencies (Figure 4-d), highest elasticity and ultimate stress were reached with FS PLA_{50}PLU200/s-PLA-fN3 75/25. It may be explained by the combination of efficient crosslinking and good balance between long and short polymer chains.

Surprisingly, in the hydrated state at 37°C, Young's modulus and ultimate stress of fibrous scaffolds were always higher than in dry state, whereas elastic limit and ultimate strain were lower than in dry state (Fig. A.8). This may appear counterintuitive considering the well-know plasticizing effect of water However, these results could be assigned to microphase separation phenomena that have recently been reported in literature for PLA-*b*-PEG-*b*-PLA copolymers. In more details, PEG blocks (more flexible, lower transition temperature) have an initial role of plasticizer for the blend, but PEG segments a prone to migration upon water uptake, which results microphase separation and stiffening [50]. In our case, due to the core-shell structure of the crosslinked fibers (crosslinked shell, uncrosslinked core see degradation), this phenomenon may overshadow the impact of the crosslinking in the hydrated state.

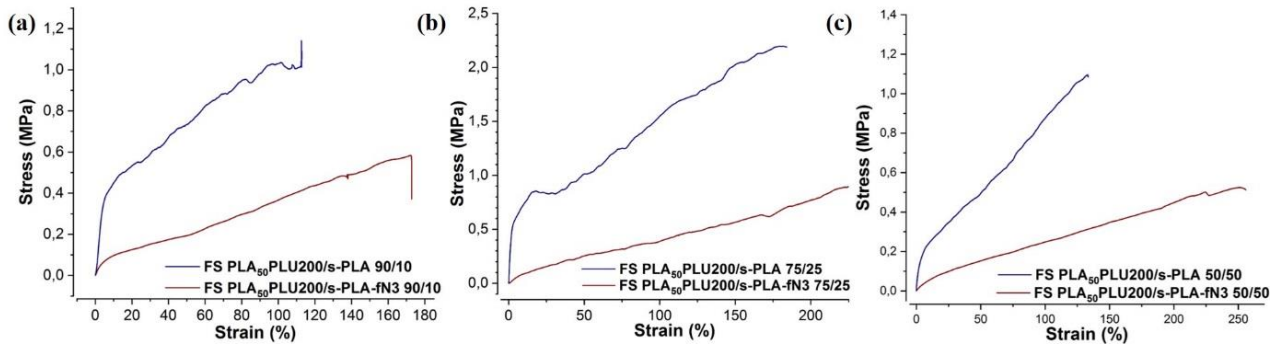

Figure 8: Mechanical tensile properties of UV-cured fibrous scaffolds based on PLA_{50}-PLU200/s-PLA-fN3 and uncured fibrous scaffolds based on PLA_{50}-PLU200/s-PLA at different ratios (a) 90/10; (b) 75/25; (c) 50/50.

3.4.4 Degradation

Scaffolds degradation was followed over 1 month (Figure 9-a). As expected, non-crosslinked fibrous scaffolds showed a faster degradation (remaining mass from 65% to 85%) compared to their crosslinked counterparts (remaining mass from 90% to 95%). Only FS with high content of PLA_{50}-PLU200 (90/10) exhibited similar degradation profiles with almost no degradation over 1 month (weight loss < 2%). It was also observed that the higher star-block copolymer (s-PLA and s-PLA-fN3) content, the faster the weight loss. This is due to the hydrophilic segments of PEG that favor water uptake (Fig. A.9) of FS (150 – 300%), which promotes their hydrolytic degradation. Interestingly, degradation profiles of all crosslinked fibers were quasi-linear as expected for chemically crosslinked elastomers. Another difference between crosslinked and non-crosslinked fibers was the additional erosion observed for the latter, which is in agreement with the reported degradation of thermoplastic aliphatic polyesters[51]. This phenomenon is illustrated by the SEM pictures presented in Figure 9-b. The absence of erosion upon degradation for the FS PLA_{50}-PLU200/s-PLA-fN3 50/50 despite weight loss (10% after 1 month) partly confirms the core-shell structure. In fact, crosslinked networks are known to maintain their 3D shape over degradation, which is observed here. While non- or less-crosslinked core chains degrade, their diffusion through the crosslinked shell is impeded, which results in a slower weight loss. Thus, UV-curing of the electropsun fibrous scaffolds allows one to modulate the degradation profile and may be useful to fit the properties of the scaffolds in the frame of soft-tissue engineering applications.

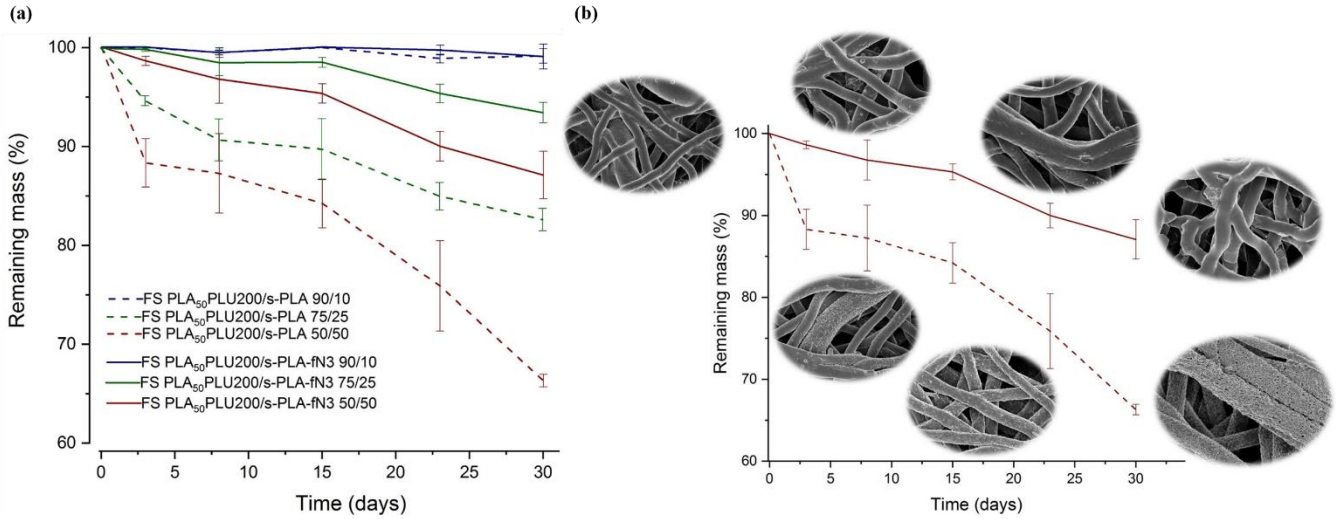

Figure 9: Evaluation of scaffold degradation (a) remaining mass during degradation time for fibrous scaffolds in PBS at 37°C. Data correspond to measurement in triplicate; (b) SEM images of PLA_{50}-PLU200/s-PLA or PLA_{50}-PLU200/s-PLA-fN3 50/50 over degradation time in PBS at 37°C, magnifications X5000. (Data are expressed as means ± SD and correspond to measurements with n = 3).

3.4.5 Cytocompatibility study

Finally, following the mechanical and degradation studies of the fibrous scaffolds, one last mandatory step to validate their potential for use with cells is the validation of their cytocompatibility. The different copolymers PLA, PluronicF127 and PEG have already been approved by FDA[4,52]. However, residual unreacted s-PLA-fN3 inside fibers may leach out from the fibers. For this reason, the cytotoxicity of the scaffolds was assessed on extracts following ISO 10993-12 recommendations. The extracts from scaffolds, C- and C+ were added on L929 fibroblasts seeded into wells and cytotoxicity was evaluated over a 24 hours period.

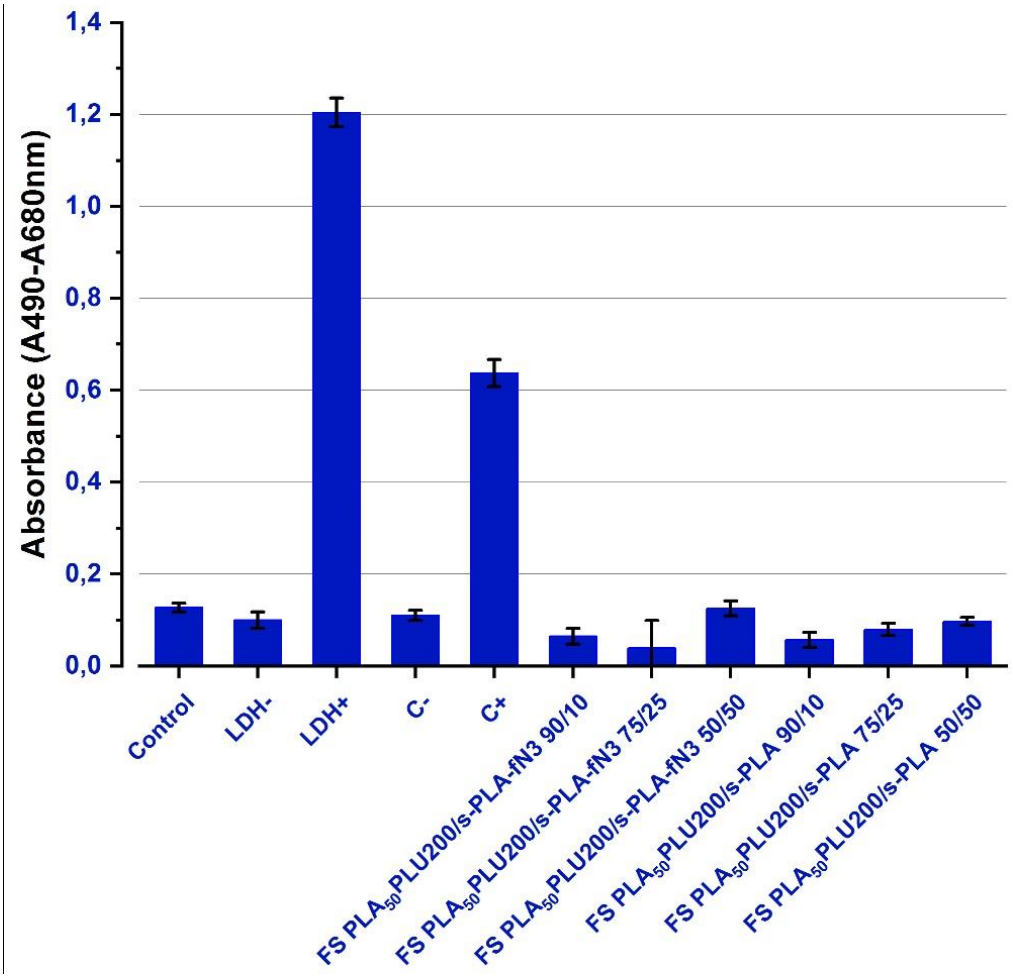

Figure 10: Cytotoxicity assessed on L929 cells after treatment with extracts of fibrous scaffolds based on PLA_{50}-PLU200/s-PLA or PLA_{50}-PLU200/s-PLA-fN3 at different ratios for 24h. (Data are expressed as means ± SD and correspond to measurements with n = 9 per condition).

Only extracts from positive control films (C+) gave around 45-50% of cytotoxicity on L929 cells. Results showed the absence of cytotoxicity of the extracts in contact with L929 cells even with extracts from the scaffolds containing the highest s-PLA-fN3 concentration (50/50). Thus, this preliminary assay confirmed the potential of the proposed degradable elastomeric biomaterials for cell-contacting applications, whose cytocompatibility will be further investigated in future dedicated work.

4 Conclusion

Triblock copolymers PLA_{50}PLU(50-200) were mixed with 2,6-bis(azidobenzylidene)-4-methylcyclohexanone (BA). BA showed low potential as photo-crosslinker with gel fractions below 15%. On the opposite, the new degradable macromolecular multifunctional (aryl azide) photo-crosslinker based on 8-arm star-block PEG-PLA copolymer (s-PLA-fN_3) yielded up to

55% gel fraction, even at lower aryl-azide concentrations compared to the molecular bis(aryl-azide) BA. This allowed the production of elastomeric fibrous scaffolds based on PLA_{50}PLU200/s-PLA-fN3 (90/10, 75/25, and 50/50 w/w) by electrospinning process. Photo-crosslinking of PLA_{50}-PLU200 by s-PLA-fN3 yielded biomaterials with enhanced elastomeric properties increased with elastic limits as high as 182%, while guarantying a modulation of the degradation kinetics. We therefore think that the proposed s-PLA-fN3 will be useful for the development of original degradable and elastomeric scaffolds for soft-tissue reconstruction. In addition, we believe that the concept of star-shaped multi-(aryl azide) copolymer could be easily applied to other applications and process thanks to the tunability offered by the macomolecular nature of this type of photo-crosslinker.

Acknowledgments

This work was supported by ANR2016-BIOSCAFF (ANR-16-CE09-0024) hold by the University of Grenoble-Alpes and the University of Montpellier. The authors wish also to acknowledge the support from the Chemistry Platform of IEM Laboratory of the Balard Chemistry pole in Montpellier, on which SEM observations analysis have been performed. We also acknowledge the help of Didier Cot (IEM, Montpellier, France) for the observation of fibrous scaffolds by SEM. ‘‘Laboratoire Rhéologie et Procédés’’ (LRP) is a part of the LabEx Tec 21 (Investissements d'Avenir – grant agreement n° ANR-11-LABX-0030) and participate to the Institut Carnot PolyNat.

Appendix A. Supplementary data

Supplementary data related to this article can be found online.

Data availability

The raw/processed data required to reproduce these findings are available upon request from the authors.

Reference

[1] H. Tian, Z. Tang, X. Zhuang, X. Chen, X. Jing, Biodegradable synthetic polymers: Preparation, functionalization and biomedical application, Prog. Polym. Sci. 37 (2012) 237–280. doi:10.1016/j.progpolymsci.2011.06.004.

[2] Y. Li, G.A. Thouas, Q.-Z. Chen, Biodegradable soft elastomers: synthesis/properties of materials and fabrication of scaffolds, RSC Adv. 2 (2012) 8229. doi:10.1039/c2ra20736b.

[3] R.P. Brannigan, A.P. Dove, Synthesis, properties and biomedical applications of hydrolytically degradable materials based on aliphatic polyesters and polycarbonates, Biomater. Sci. 5 (2017) 9–21. doi:10.1039/C6BM00584E.

[4] Q. Chen, S. Liang, G.A. Thouas, Elastomeric biomaterials for tissue engineering, Prog. Polym. Sci. 38 (2013) 584–671. doi:10.1016/j.progpolymsci.2012.05.003.

[5] X. Lee, M.U. Wahit, N. Adrus, Biodegradable and temperature-responsive thermoset polyesters with renewable monomers, J. Appl. Polym. Sci. 133 (2016). doi:10.1002/app.44007.

[6] M. Basko, M. Bednarek, L. Vlaminck, P. Kubisa, F.E. Du Prez, Biodegradable polymer networks via triazolinedione-crosslinking of oleyl-functionalized poly(ε-caprolactone), Eur. Polym. J. 89 (2017) 230–240. doi:10.1016/j.eurpolymj.2017.02.031.

[7] M.A. Tasdelen, Diels–Alder "click" reactions: recent applications in polymer and material science, Polym. Chem. 2 (2011) 2133. doi:10.1039/c1py00041a.

[8] M. Gonzalez-Burgos, A. Latorre-Sanchez, J.A. Pomposo, Advances in single chain technology, Chem. Soc. Rev. 44 (2015) 6122–6142. doi:10.1039/C5CS00209E.

[9] M. Claudino, I. van der Meulen, S. Trey, M. Jonsson, A. Heise, M. Johansson, Photoinduced thiol-ene crosslinking of globalide/ε-caprolactone copolymers: Curing performance and resulting thermoset properties, J. Polym. Sci. Part Polym. Chem. 50 (2012) 16–24. doi:10.1002/pola.24940.

[10] A. Concellón, L. Asín, S. González-Lana, J.M. de la Fuente, C. Sánchez-Somolinos, M. Piñol, L. Oriol, Photopolymers based on ethynyl-functionalized degradable polylactides by thiol-yne 'Click Chemistry,' Polymer. 117 (2017) 259–267. doi:10.1016/j.polymer.2017.04.035.

[11] B. Nottelet, G. Tambutet, Y. Bakkour, J. Coudane, Redox and thiol–ene cross-linking of mercapto poly(ε-caprolactone) for the preparation of reversible degradable elastomeric materials, Polym. Chem. 3 (2012) 2956. doi:10.1039/c2py20436c.

[12] C. Lorenzini, D.L. Versace, J. Babinot, E. Renard, V. Langlois, Biodegradable hybrid poly(3-hydroxyalkanoate)s networks through silsesquioxane domains formed by efficient UV-curing, React. Funct. Polym. 84 (2014) 53–59. doi:10.1016/j.reactfunctpolym.2014.09.008.

[13] J. Jansen, M.P. Tibbe, G. Mihov, J. Feijen, D.W. Grijpma, Photo-crosslinked networks prepared from fumaric acid monoethyl ester-functionalized poly(d,l-lactic acid) oligomers and N-vinyl-2-pyrrolidone for the controlled and sustained release of proteins, Acta Biomater. 8 (2012) 3652–3659. doi:10.1016/j.actbio.2012.06.011.

[14] J. Yu, X. Xu, F. Yao, Z. Luo, L. Jin, B. Xie, S. Shi, H. Ma, X. Li, H. Chen, In situ covalently cross-linked PEG hydrogel for ocular drug delivery applications, Int. J. Pharm. 470 (2014) 151–157. doi:10.1016/j.ijpharm.2014.04.053.

[15] Y.-C. Yeh, L. Ouyang, C.B. Highley, J.A. Burdick, Norbornene-modified poly(glycerol sebacate) as a photocurable and biodegradable elastomer, Polym. Chem. 8 (2017) 5091–5099. doi:10.1039/C7PY00323D.

[16] S.N. Sheikholeslami, M. Rafizadeh, F.A. Taromi, H. Shirali, E. Jabbari, Material properties of degradable Poly(butylene succinate- co -fumarate) copolymer networks synthesized by polycondensation of pre-homopolyesters, Polymer. 98 (2016) 70–79. doi:10.1016/j.polymer.2016.06.012.

[17] Q. Liu, L. Jiang, R. Shi, L. Zhang, Synthesis, preparation, in vitro degradation, and application of novel degradable bioelastomers—A review, Prog. Polym. Sci. 37 (2012) 715–765. doi:10.1016/j.progpolymsci.2011.11.001.

[18] E. Bat, B.H.M. Kothman, G.A. Higuera, C.A. van Blitterswijk, J. Feijen, D.W. Grijpma, Ultraviolet light crosslinking of poly(trimethylene carbonate) for elastomeric tissue engineering scaffolds, Biomaterials. 31 (2010) 8696–8705. doi:10.1016/j.biomaterials.2010.07.102.

[19] C. Mangeon, E. Renard, F. Thevenieau, V. Langlois, Networks based on biodegradable polyesters: An overview of the chemical ways of crosslinking, Mater. Sci. Eng. C. 80 (2017) 760–770. doi:10.1016/j.msec.2017.07.020.

[20] B. Rupp, C. Ebner, E. Rossegger, C. Slugovc, F. Stelzer, F. Wiesbrock, UV-induced crosslinking of the biopolyester poly(3-hydroxybutyrate)-co-(3-hydroxyvalerate), Green Chem. 12 (2010) 1796. doi:10.1039/c0gc00066c.

[21] M. Avadanei, Photochemistry of 2,6-di(4′-azidobenzylidene)-methylcyclohexanone in polymer matrices, J. Appl. Polym. Sci. 134 (2017). doi:10.1002/app.44694.

[22] G.W. Preston, A.J. Wilson, Photo-induced covalent cross-linking for the analysis of biomolecular interactions, Chem. Soc. Rev. 42 (2013) 3289. doi:10.1039/c3cs35459h.

[23] N. Yasuda, S. Yamamoto, Y. Wada, S. Yanagida, Photocrosslinking reaction of vinyl-functional polyphenylsilsesquioxane sensitized with aromatic bisazide compounds, J. Polym. Sci. Part Polym. Chem. 39 (2001) 4196–4205. doi:10.1002/pola.10065.

[24] J. Jia, G.L. Baker, Cross-linking of poly[1-(trimethylsilyl)-1-propyne] membranes using bis(aryl azides), J. Polym. Sci. Part B Polym. Phys. 36 (1998) 959–968. doi:10.1002/(SICI)1099-0488(19980430)36:6<959::AID-POLB3>3.0.CO;2-B.

[25] M. Xie, J. Ge, B. Lei, Q. Zhang, X. Chen, P.X. Ma, Star-Shaped, Biodegradable, and Elastomeric PLLA-PEG-POSS Hybrid Membrane With Biomineralization Activity for Guiding Bone Tissue Regeneration: Star-Shaped, Biodegradable, and Elastomeric…, Macromol. Biosci. 15 (2015) 1656–1662. doi:10.1002/mabi.201500237.

[26] M. Xie, J. Ge, Y. Xue, Y. Du, B. Lei, P.X. Ma, Photo-crosslinked fabrication of novel biocompatible and elastomeric star-shaped inositol-based polymer with highly tunable mechanical behavior and degradation, J. Mech. Behav. Biomed. Mater. 51 (2015) 163–168. doi:10.1016/j.jmbbm.2015.07.011.

[27] P. Zhao, H. Gu, H. Mi, C. Rao, J. Fu, L. Turng, Fabrication of scaffolds in tissue engineering: A review, Front. Mech. Eng. 13 (2018) 107–119. doi:10.1007/s11465-018-0496-8.

[28] Udayabhanu Jammalamadaka, Karthik Tappa, Recent Advances in Biomaterials for 3D Printing and Tissue Engineering, J. Funct. Biomater. 9 (2018) 22. doi:10.3390/jfb9010022.

[29] M. Boffito, S. Sartori, G. Ciardelli, Polymeric scaffolds for cardiac tissue engineering: requirements and fabrication technologies: Polymeric scaffolds for cardiac tissue engineering, Polym. Int. 63 (2014) 2–11. doi:10.1002/pi.4608.

[30] M. Kitsara, P. Joanne, S.E. Boitard, I. Ben Dhiab, B. Poinard, P. Menasché, C. Gagnieu, P. Forest, O. Agbulut, Y. Chen, Fabrication of cardiac patch by using electrospun collagen fibers, Microelectron. Eng. 144 (2015) 46–50. doi:10.1016/j.mee.2015.02.034.

[31] J.R. Dias, P.L. Granja, P.J. Bártolo, Advances in electrospun skin substitutes, Prog. Mater. Sci. 84 (2016) 314–334. doi:10.1016/j.pmatsci.2016.09.006.

[32] O.I. Kalaoglu-Altan, R. Sanyal, A. Sanyal, Reactive and 'clickable' electrospun polymeric nanofibers, Polym. Chem. 6 (2015) 3372–3381. doi:10.1039/C5PY00098J.

[33] A. Lancuški, S. Fort, F. Bossard, Electrospun Azido-PCL Nanofibers for Enhanced Surface Functionalization by Click Chemistry, ACS Appl. Mater. Interfaces. 4 (2012) 6499–6504. doi:10.1021/am301458y.

[34] M.W. Thielke, E.P. Bruckner, D.L. Wong, P. Theato, Thiol-ene modification of electrospun polybutadiene fibers crosslinked by UV irradiation, Polymer. 55 (2014) 5596–5599. doi:10.1016/j.polymer.2014.09.002.

[35] I. Stefani, J.J. Cooper-White, Development of an in-process UV-crosslinked, electrospun PCL/aPLA-co-TMC composite polymer for tubular tissue engineering applications, Acta Biomater. 36 (2016) 231–240. doi:10.1016/j.actbio.2016.03.013.

[36] F. Chen, G. Hochleitner, T. Woodfield, J. Groll, P.D. Dalton, B.G. Amsden, Additive Manufacturing of a Photo-Cross-Linkable Polymer via Direct Melt Electrospinning Writing for Producing High Strength Structures, Biomacromolecules. 17 (2016) 208–214. doi:10.1021/acs.biomac.5b01316.

[37] A. Leroy, C. Pinese, C. Bony, X. Garric, D. Noël, B. Nottelet, J. Coudane, Investigation on the properties of linear PLA-poloxamer and star PLA-poloxamine copolymers for temporary biomedical applications, Mater. Sci. Eng. C. 33 (2013) 4133–4139. doi:10.1016/j.msec.2013.06.001.

[38] A. Leroy, B. Nottelet, C. Bony, C. Pinese, B. Charlot, X. Garric, D. Noël, J. Coudane, PLA-poloxamer/poloxamine copolymers for ligament tissue engineering: sound macromolecular design for degradable scaffolds and MSC differentiation, Biomater. Sci. 3 (2015) 617–626. doi:10.1039/C4BM00433G.

[39] C. Pinese, A. Leroy, B. Nottelet, C. Gagnieu, J. Coudane, X. Garric, Rolled knitted scaffolds based on PLA-pluronic copolymers for anterior cruciate ligament reinforcement: A step by step conception: rolled knitted scaffolds, J. Biomed. Mater. Res. B Appl. Biomater. 105 (2017) 735–743. doi:10.1002/jbm.b.33604.

[40] S. Nedjari, G. Schlatter, A. Hébraud, Thick electrospun honeycomb scaffolds with controlled pore size, Mater. Lett. 142 (2015) 180–183. doi:10.1016/j.matlet.2014.11.118.

[41] F. Bossard, N. El Kissi, A. D'Aprea, F. Alloin, J.-Y. Sanchez, A. Dufresne, Influence of dispersion procedure on rheological properties of aqueous solutions of high molecular weight PEO, Rheol. Acta. 49 (2010) 529–540. doi:10.1007/s00397-009-0402-8.

[42] A. Schulz, A. Stocco, A. Bethry, J.-P. Lavigne, J. Coudane, B. Nottelet, Direct Photomodification of Polymer Surfaces: Unleashing the Potential of Aryl-Azide Copolymers, Adv. Funct. Mater. 28 (2018) 1800976. doi:10.1002/adfm.201800976.

[43] V. Pourcelle, S. Devouge, M. Garinot, V. Préat, J. Marchand-Brynaert, PCL−PEG-Based Nanoparticles Grafted with GRGDS Peptide: Preparation and Surface Analysis by XPS, Biomacromolecules. 8 (2007) 3977–3983. doi:10.1021/bm700841y.

[44] L. Wei, A.G. McDonald, Accelerated weathering studies on the bioplastic, poly(3-hydroxybutyrate- co -3-hydroxyvalerate), Polym. Degrad. Stab. 126 (2016) 93–100. doi:10.1016/j.polymdegradstab.2016.01.023.

[45] O. Suwantong, Biomedical applications of electrospun polycaprolactone fiber mats: Biomedical Applications of Electrospun Polycaprolactone Fiber Mats, Polym. Adv. Technol. 27 (2016) 1264–1273. doi:10.1002/pat.3876.

[46] N. Masoumi, D. Copper, P. Chen, A. Cubberley, K. Guo, R.-Z. Lin, B. Ahmed, D. Martin, E. Aikawa, J. Melero-Martin, J. Mayer, Elastomeric Fibrous Hybrid Scaffold Supports In Vitro and In Vivo Tissue Formation, Adv. Funct. Mater. 27 (2017) 1606614. doi:10.1002/adfm.201606614.

[47] E. Mazza, A.E. Ehret, Mechanical biocompatibility of highly deformable biomedical materials, J. Mech. Behav. Biomed. Mater. 48 (2015) 100–124. doi:10.1016/j.jmbbm.2015.03.023.

[48] S. Mohammadzadehmoghadam, Y. Dong, I. Jeffery Davies, Recent progress in electrospun nanofibers: Reinforcement effect and mechanical performance, J. Polym. Sci. Part B Polym. Phys. 53 (2015) 1171–1212. doi:10.1002/polb.23762.

[49] J. Fernández, O. Auzmendi, H. Amestoy, A. Diez-Torre, J.-R. Sarasua, Mechanical properties and fatigue analysis on poly(ε-caprolactone)-polydopamine-coated nanofibers and poly(ε-caprolactone)-carbon nanotube composite scaffolds, Eur. Polym. J. 94 (2017) 208–221. doi:10.1016/j.eurpolymj.2017.07.013.

[50] M. Wang, D. Yuan, X. Fan, N.G. Sahoo, C. He, Polymer Nanocomposite Hydrogels Exhibiting Both Dynamic Restructuring and Unusual Adhesive Properties, Langmuir. 29 (2013) 7087–7095. doi:10.1021/la401269p.

[51] M. Vert, Degradable and bioresorbable polymers in surgery and in pharmacology: beliefs and facts, J. Mater. Sci. Mater. Med. 20 (2009) 437–446. doi:10.1007/s10856-008-3581-4.

[52] S. Rupnik, S. Buwalda, S. Dejean, A. Bethry, X. Garric, J. Coudane, B. Nottelet, Redox Reducible and Hydrolytically Degradable PEG-PLA Elastomers as Biomaterial for Temporary Drug-Eluting Medical Devices, Macromol. Biosci. 16 (2016) 1792–1802. doi:10.1002/mabi.201600132.

Appendix

Degradable multi(aryl-azide) star copolymer as universal photo-crosslinker for elastomeric scaffolds

Louis Gangolphe[a,b], Stéphane Déjean[a], Audrey Bethry[a], Sylvie Hunger[a], Coline Pinese[a], Xavier Garric[a], Frédéric Bossard[b], Benjamin Nottelet[a]*

[a]*Department of Artificials Biopolymers, Max Mousseron Institute of Biomolecules (IBMM), UMR CNRS 5247, University of Montpellier, France*

[b]*Univ. Grenoble Alpes, CNRS, Grenoble INP*, LRP, 38000 Grenoble, France * Institute of Engineering Univ. Grenoble Alpes*

[*]*benjamin.nottelet@umontpellier.fr*

- ^{1}H NMR spectrum of triblock copolymer
- ^{1}H NMR spectrum of aryl-azide functionalized triblock copolymer
- UV lamp emission spectrum
- Temperature evolution inside the Dymax UV device
- Influence of Influence of the type of UV-bulb (MB vs. MHB) on gel fraction
- FTIR analysis of scaffolds before and after UV irradiation and influence of UV-bulb (MB vs. MHB)
- DSC analysis of star-shaped copolymer s-PLA(-fN3)
- Mechanical tensile properties of UV-cured fibrous scaffolds
- Water uptake of fibrous scaffolds

Appendix 1 (A.1)

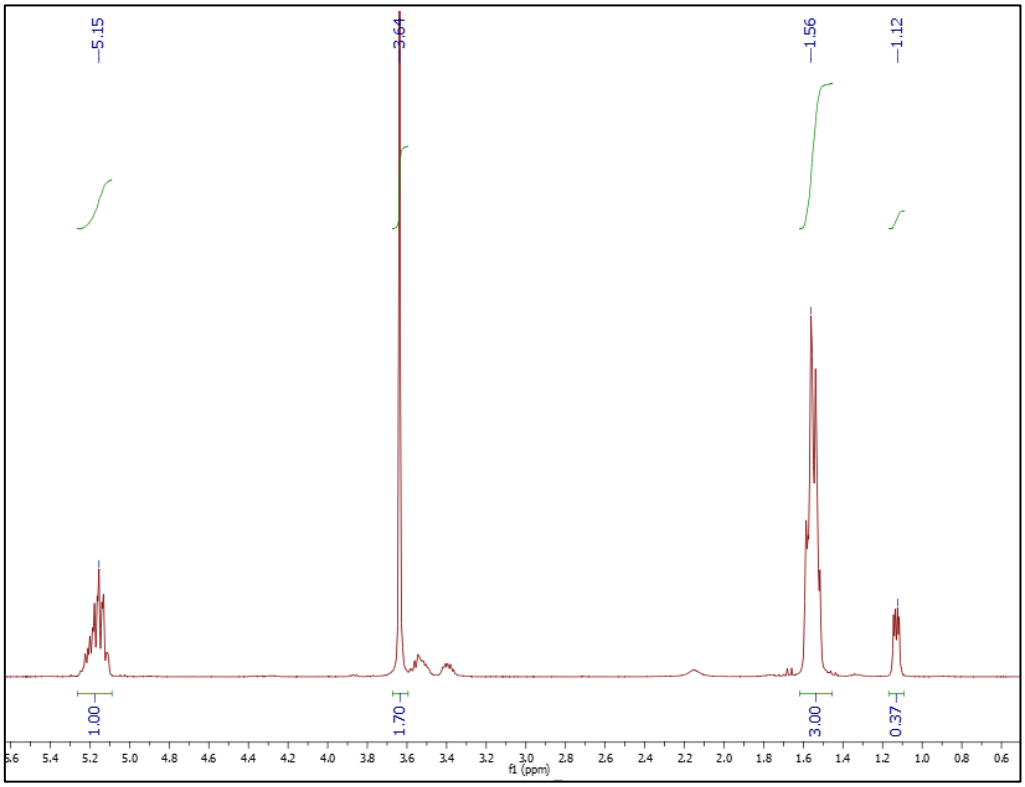

Figure A.11: Typical ^{1}H NMR spectra of PLA_{50}-Pluronic®F127-PLA_{50} (PLA_{50}PLU 50, 50 000 $g.mol^{-1}$)

Appendix 2 (A.2)

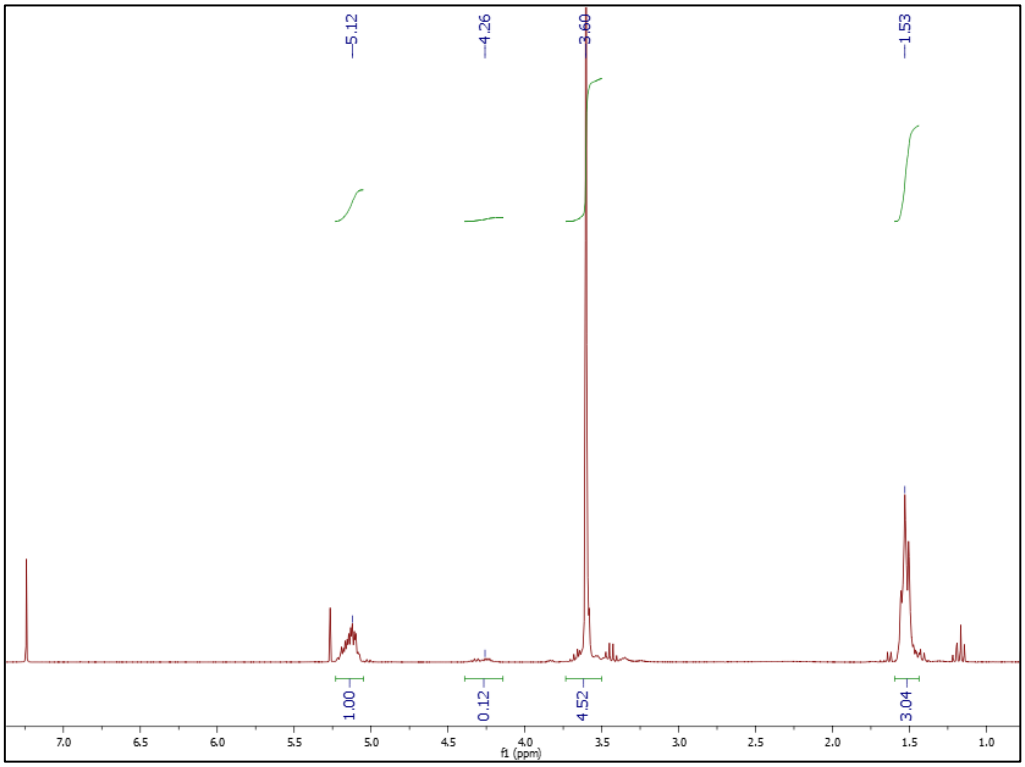

Figure A.2: ^{1}H NMR spectra of $PEG_{8arm}10k\text{-}PLA_{94}$ (s-PLA).

Appendix 3 (A.3)

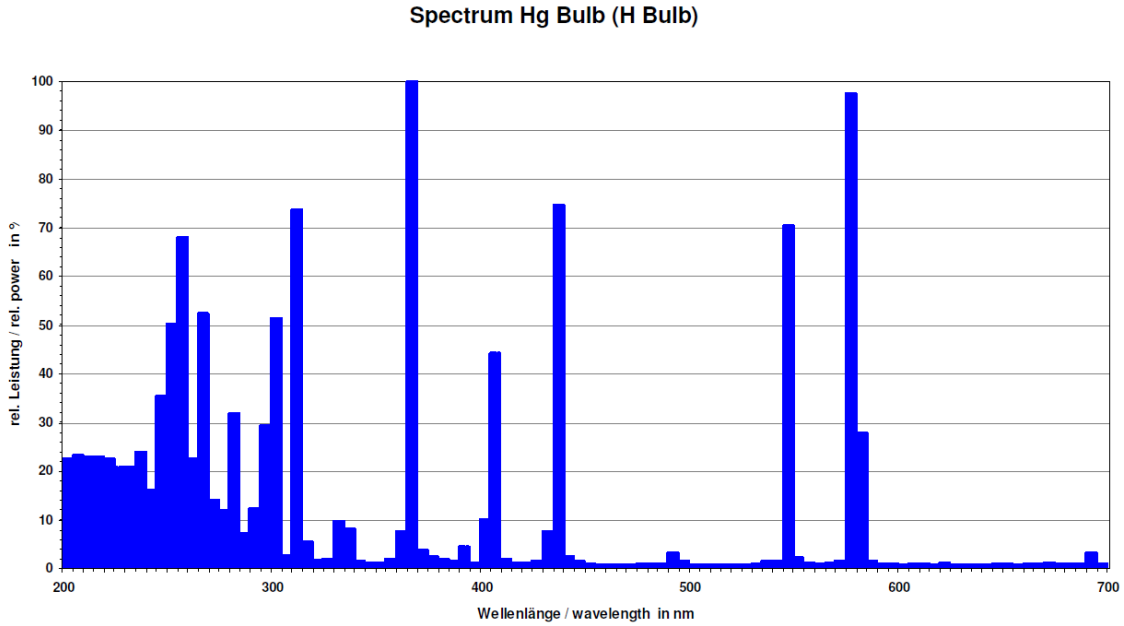

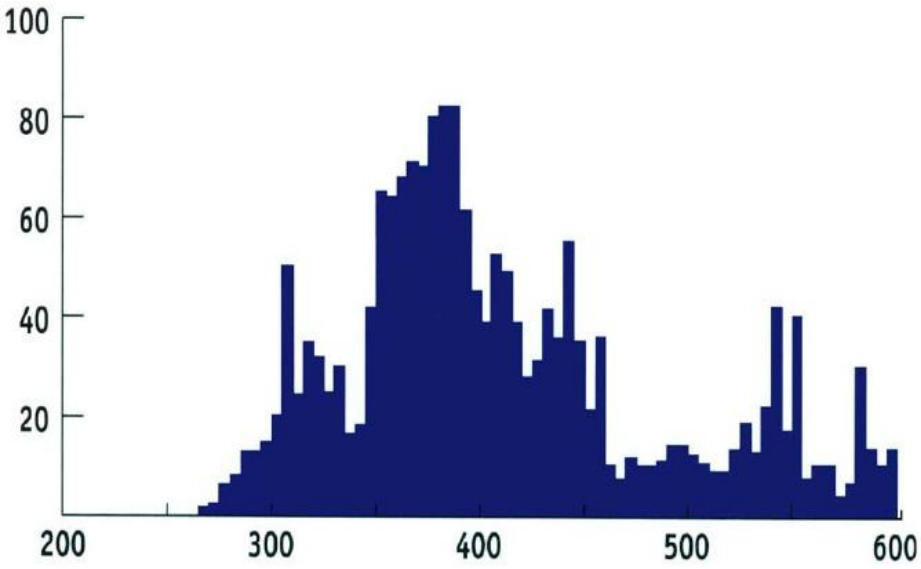

Figure A.3: (a) Mercury bulb emission spectrum; (b) Metal halide bulb emission spectrum (data from supplier DYMAX COORPORATION , https://dymax.com)

Appendix 4 (A.4)

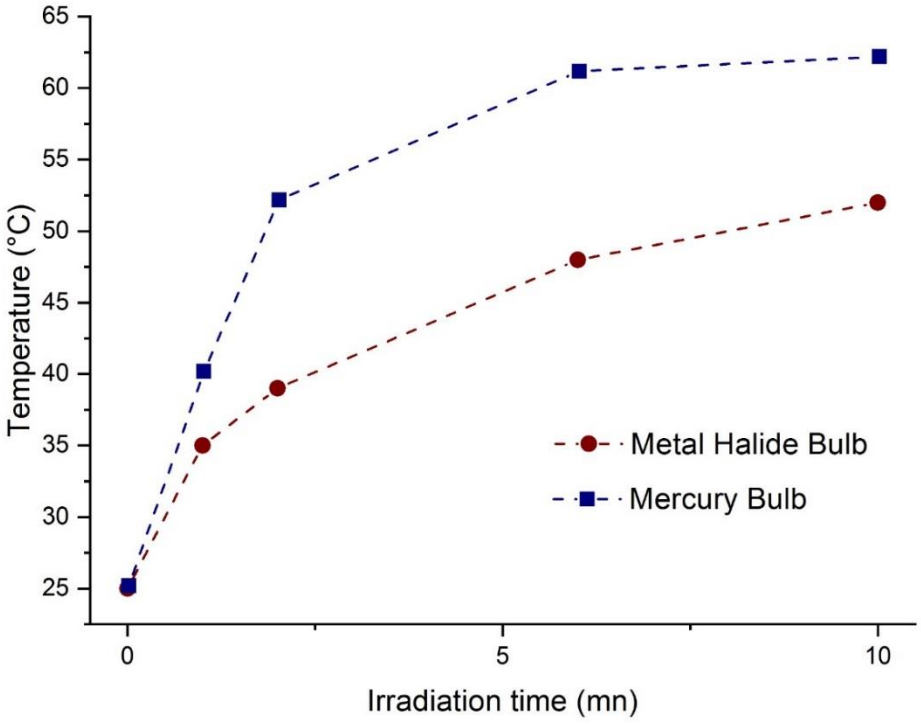

Figure A.4: Influence of UV-bulbs on the temperature inside the enclosure of Dymax device

Appendix 5 (A.5)

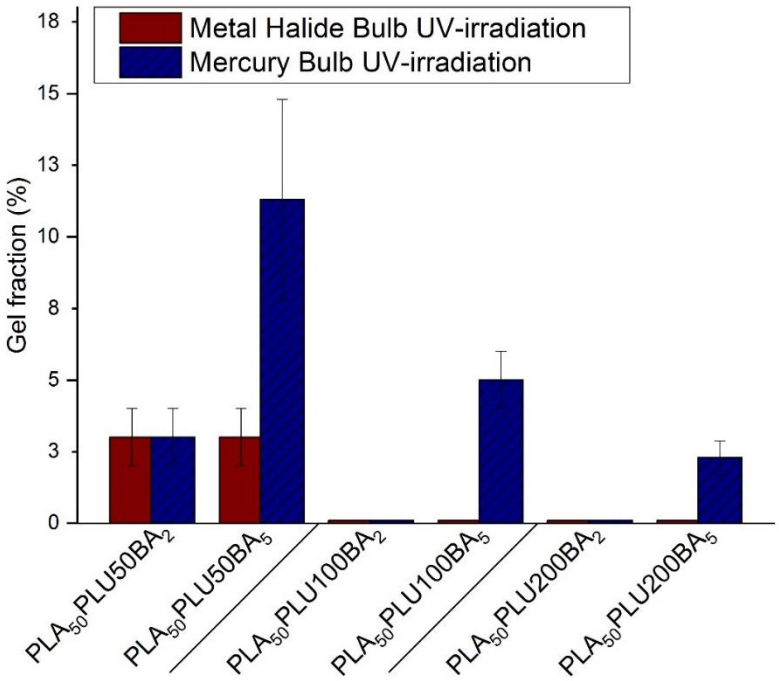

Figure A.5: Influence of the type of UV-bulb (MB vs. MHB) used to generate the elastomers evaluated by gel fraction analysis

Appendix 6 (A.6)

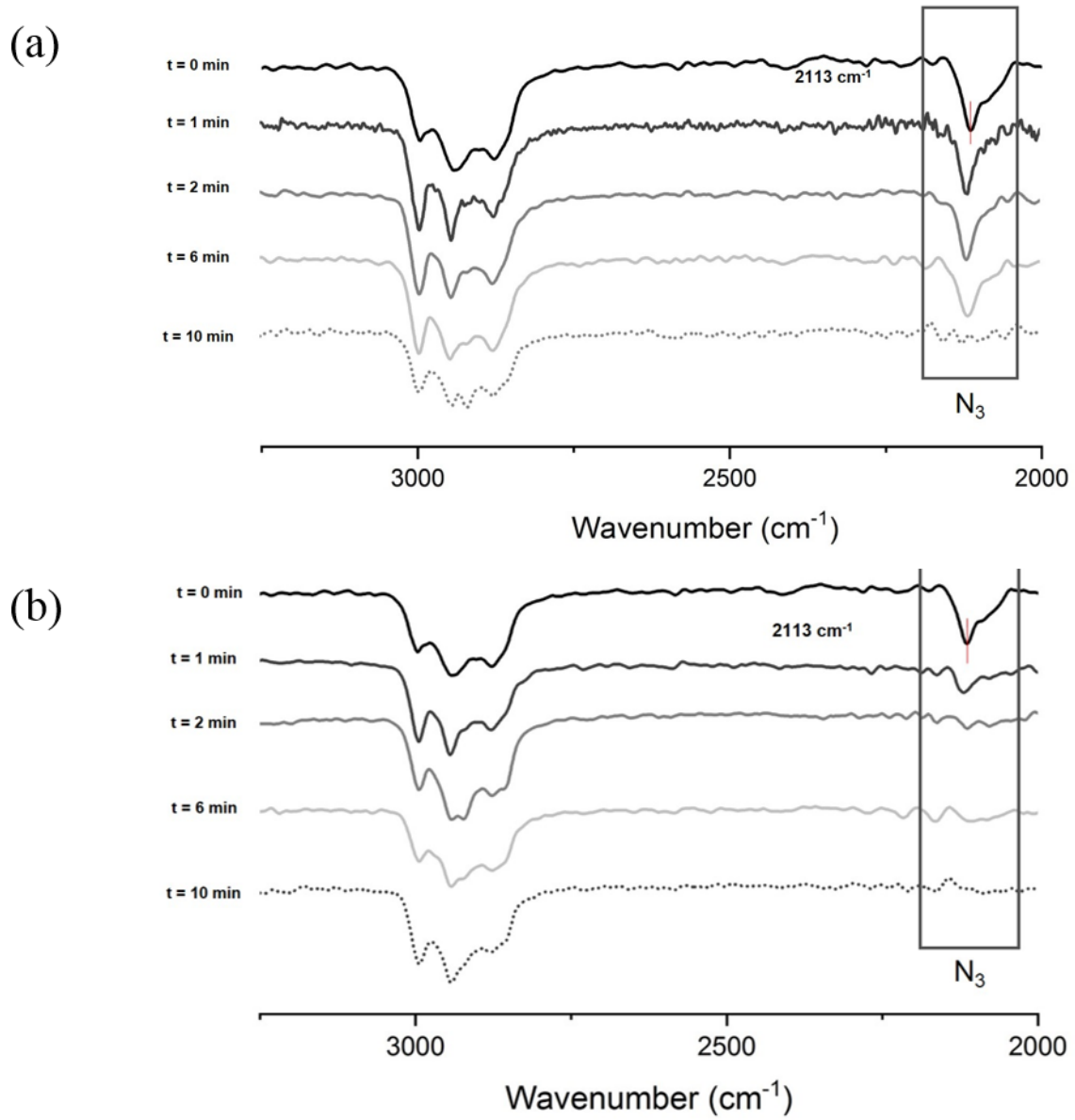

Figure A.6: FTIR analysis of scaffolds before and after UV irradiation at different time with two different UV-bulb: (a) Metal Halide Bulb and (b) Mercury Bulb. The photo-activation of aromatic biazide generating nitrene was showed by the loss of the characteristic azide IR band located at 2110 cm-1.

Appendix 7 (A.7)

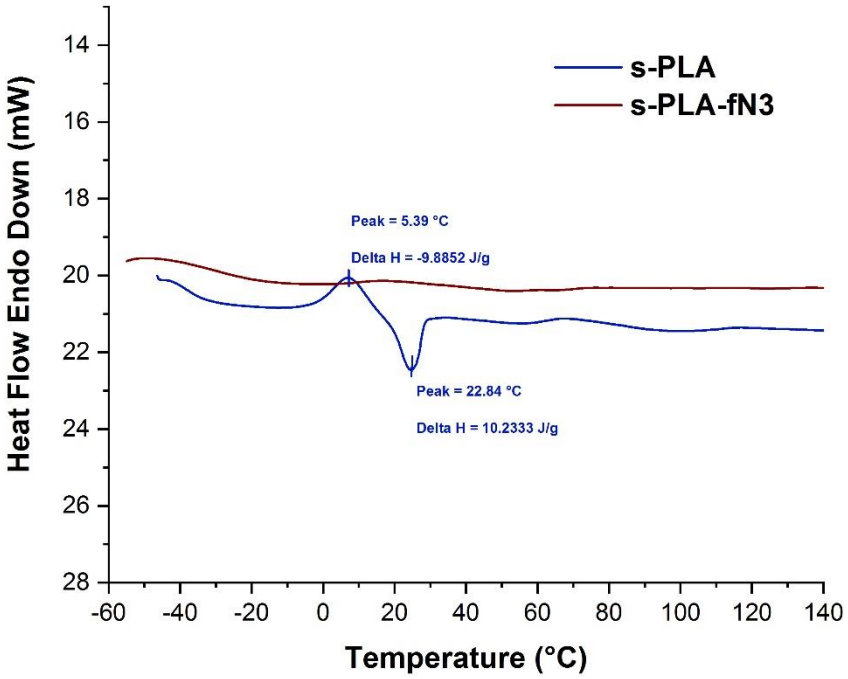

Figure A.7: DSC analysis of star-shaped copolymer s-PLA and s-PLA-fN3

Appendix 8 (A.8)

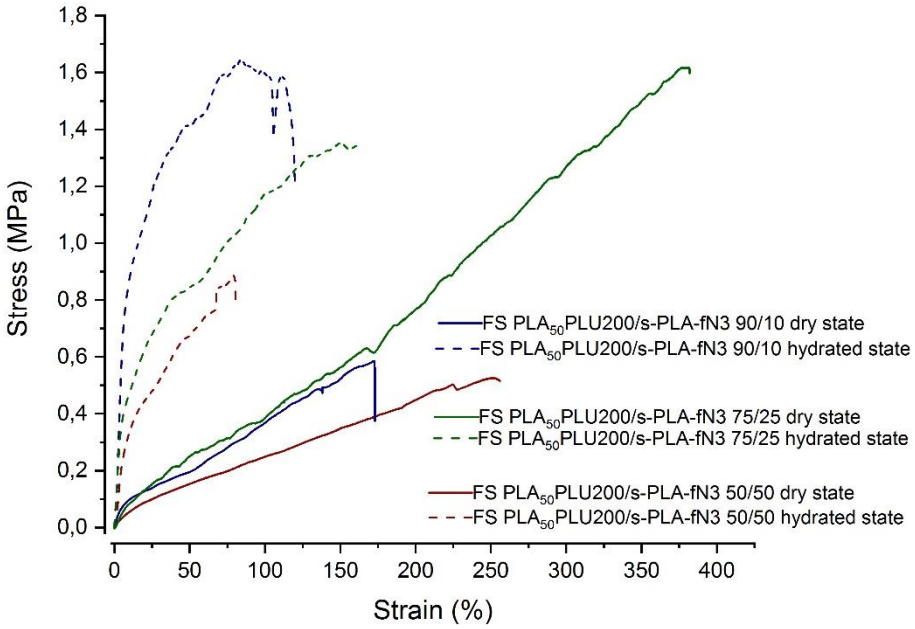

Figure A.8: Mechanical tensile properties of UV-cured fibrous scaffolds based on PLA_{50}-PLU200/s-PLA-fN3 in hydrated and dry state at 37°C

Appendix 9 (A.9)

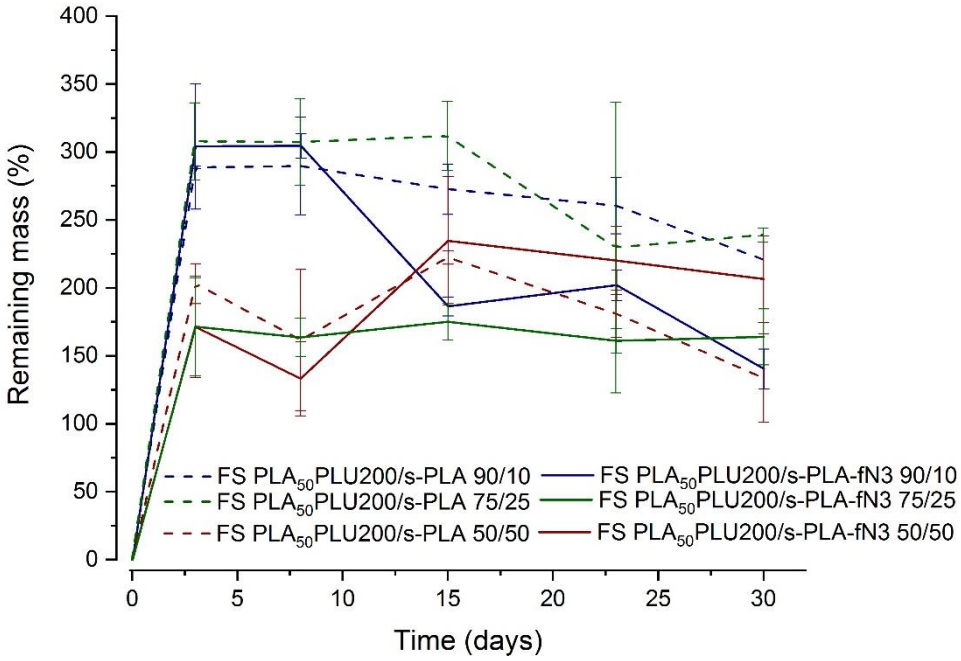

Figure A.9: Water uptake of fibrous scaffolds based on PLA_{50}-PLU200/s-PLA or PLA_{50}-PLU200/s-PLA-fN3 at different ratios